

Role of Mossy Fiber Sprouting and Mossy Cell Loss in Hyperexcitability: A Network Model of the Dentate Gyrus Incorporating Cell Types and Axonal Topography

Vijayalakshmi Santhakumar, Ildiko Aradi, and Ivan Soltesz

Department of Anatomy and Neurobiology, University of California, Irvine, California

Submitted 30 July 2004; accepted in final form 31 August 2004

Santhakumar, Vijayalakshmi, Ildiko Aradi, and Ivan Soltesz. Role of mossy fiber sprouting and mossy cell loss in hyperexcitability: a network model of the dentate gyrus incorporating cell types and axonal topography. *J Neurophysiol* 93: 437–453, 2005. First published September 1, 2004; doi:10.1152/jn.00777.2004. Mossy cell loss and mossy fiber sprouting are two characteristic consequences of repeated seizures and head trauma. However, their precise contributions to the hyperexcitable state are not well understood. Because it is difficult, and frequently impossible, to independently examine using experimental techniques whether it is the loss of mossy cells or the sprouting of mossy fibers that leads to dentate hyperexcitability, we built a biophysically realistic and anatomically representative computational model of the dentate gyrus to examine this question. The 527-cell model, containing granule, mossy, basket, and hilar cells with axonal projections to the perforant-path termination zone, showed that even weak mossy fiber sprouting (10–15% of the strong sprouting observed in the pilocarpine model of epilepsy) resulted in the spread of seizure-like activity to the adjacent model hippocampal laminae after focal stimulation of the perforant path. The simulations also indicated that the spatially restricted, lamellar distribution of the sprouted mossy fiber contacts reported in *in vivo* studies was an important factor in sustaining seizure-like activity in the network. In contrast to the robust hyperexcitability-inducing effects of mossy fiber sprouting, removal of mossy cells resulted in decreased granule cell responses to perforant-path activation in agreement with recent experimental data. These results indicate the crucial role of mossy fiber sprouting even in situations where there is only relatively weak mossy fiber sprouting as is the case after moderate concussive experimental head injury.

INTRODUCTION

Head injury is associated with a long-lasting increase in the likelihood of developing temporal lobe epilepsy (Annegers and Coan 2000; Jennett 1975). Studies using animal models of head trauma have shown that a single episode of concussive brain injury causes an increase in the excitability of dentate granule cells in response to perforant-path stimulation (Coulter et al. 1996; Lowenstein et al. 1992; Santhakumar et al. 2001, 2003; Toth et al. 1997). Although the exact mechanisms underlying the posttraumatic dentate hyperexcitability are not fully understood, experimental head injury is associated with a specific pattern of hilar cell loss (Lowenstein et al. 1992; Santhakumar et al. 2000; Toth et al. 1997) and the sprouting of recurrent excitatory collaterals by granule cell axons (Golarai et al. 2001; Santhakumar et al. 2001). These alterations are

similar to the histopathological characteristics observed in tissue from patients with temporal lobe epilepsy (Bruton 1988; Margerison and Corsellis 1966; Sutula et al. 1989; Zhang and Houser 1999).

Although the mossy fiber sprouting-related appearance of new recurrent excitatory feed-back loops is generally considered to be a plausible mechanism of hyperexcitability (Coulter 1999; Nadler 2003; Sutula et al. 1992), it is not entirely clear if even a low degree of sprouting, such as that observed after moderate experimental head injury (Santhakumar et al. 2001), is sufficient to significantly decrease the threshold for seizure-like events in the dentate gyrus. Second, it is also unclear what role the compact, lamellar distribution of the sprouted recurrent mossy fibers, observed in animal models of spontaneous recurrent seizures (Buckmaster and Dudek 1999; Buckmaster et al. 2002b), plays in the spreading of granule cell excitability because it may be hypothesized that a less spatially restricted, extra-lamellar sprouting would be more conducive to the spreading of seizure-like activity patterns.

In addition to these two major questions regarding the hyperexcitability-enhancing roles of mossy fiber sprouting, another controversial issue concerned the relative importance of the loss and survival of mossy cells from the hilus after seizures and trauma (reviewed in Ratzliff et al. 2002). Although an earlier hypothesis suggested that the central event in the development of limbic epilepsy was the excitatory denervation of surviving dentate interneurons resulting from the loss of mossy cells (Sloviter 1994), an alternative theory, named the “irritable mossy cell hypothesis,” proposed that it was not the loss but the survival of mossy cells that played a crucial role in dentate hyperexcitability (Ratzliff et al. 2002; Santhakumar et al. 2000). Recently, experiments revealed that the rapid removal of hilar mossy cells from the dentate network invariably decreased (and not increased) granule cell excitability to perforant-path stimulation (Ratzliff et al. 2004), indicating that the loss of mossy cells in itself is unlikely to directly underlie dentate hyperexcitability. In agreement with the idea that surviving mossy cells may play a role in spreading hyperexcitability through their long-range connections, hilar mossy cells that survive moderate head trauma (resulting in the loss of about half of the hilar GABAergic interneurons and half of the excitatory hilar mossy cells) do show hyperexcitable responses to perforant-path stimulation (Santhakumar et al. 2000), and hyperexcitable mossy cells have also been observed after

Address for reprint requests and other correspondence: V. Santhakumar, UCLA Neurobiology BOX 951763, 63-314 CHS Los Angeles, CA 90095-1763 (E-mail: vsanthakumar@mednet.ucla.edu).

The costs of publication of this article were defrayed in part by the payment of page charges. The article must therefore be hereby marked “advertisement” in accordance with 18 U.S.C. Section 1734 solely to indicate this fact.

pilocarpine-induced seizures (Scharfman et al. 2001). In addition, the postinjury dentate hyperexcitability is observed even after blocking GABAergic inhibition (i.e., in a fully disinhibited dentate gyrus), suggesting that the excitatory network contains the circuit sufficient to generate hyperexcitability (Santhakumar et al. 2000).

The objective of this study was to gain further mechanistic insights into the possible roles of mossy fiber sprouting and mossy cell loss in dentate excitability with particular reference to posttraumatic hyperexcitability. We employed computational models, incorporating some key structural and functional properties of the biological dentate gyrus, to address the following questions: 1) can low levels of mossy fiber sprouting underlie hyperexcitable responses of granule cells to perforant-path stimulation? 2) Does mossy cell loss aid or impede the initiation and propagation of network activity in the dentate gyrus? And 3) how does the experimentally observed axonal topography of the sprouted mossy fibers modulate the abnormal spread of network activity? The answers to these questions are likely to increase our understanding of the mechanisms underlying limbic epileptogenesis and posttraumatic dentate hyperexcitability.

METHODS

A reduced dentate network was constructed based on a 2,000:1 scaling-down of the numbers of the four major cell types in the dentate gyrus (Patton and McNaughton 1995). All simulations were performed using NEURON (Hines and Carnevale 1997) running on a PC under Redhat Linux. Model implementations of the biophysical mechanisms were obtained from <http://senselab.med.yale.edu/senselab/modeldb> and Aradi and Holmes (1999).

Construction of biophysically realistic multicompartmental models of dentate cells

We constructed multicompartmental models of the dentate granule, mossy, basket, and hilar perforant-path associated cells (HIPP cells).

The dimensions of the somatic and dendritic compartments of the model cells are presented in Table 1. Schematic representations of the model cells are illustrated in Fig. 1, A–D. The granule cell model was adapted from Aradi and Holmes (1999). The structure of the multicompartmental models of mossy, basket, and HIPP cells were developed based on morphology of the cell types reported in the literature (Bartos et al. 2001; Buckmaster et al. 1993, 2002a; Freund and Buzsaki 1996; Geiger et al. 1997).

The intrinsic properties of the cell types were modeled based on experimental data (Lubke et al. 1998; Staley et al. 1992) (note that these data were obtained in the presence of blockers of synaptic activity). The passive membrane parameters and source and densities of active conductances in the somatic compartment of the model cells are listed in Table 2. For granule cells, the somato-dendritic distribution of active conductances was adapted from Aradi and Holmes (1999). In all other cell types, the active conductances, with the exception of sodium and fast delayed rectifier potassium channels, were distributed uniformly in all compartments. Sodium and fast delayed rectifier potassium conductances were present only in the soma and proximal dendritic compartments. Additionally, because granule cells (Desmond and Levy 1985) and mossy cells (Amaral 1978) are rich in dendritic spines, we corrected for the membrane area contribution of dendritic spines (Rall et al. 1992). For granule cells, correction for the membrane contribution of spines was performed by decreasing membrane resistivity (increasing leak conductance to $63 \mu\text{S}/\text{cm}^2$) and increasing the capacitance to $1.6 \mu\text{F}/\text{cm}^2$ (Aradi and Holmes 1999). In the case of mossy cells, because they share several structural and functional properties with CA3 pyramidal cells (Buckmaster et al. 1993), spine density estimates from CA3 cells (Hama et al. 1994) were used to estimate the contribution of spines to the membrane. Specifically, the dendritic leak conductance ($44 \mu\text{S}/\text{cm}^2$) and capacitance ($2.4 \mu\text{F}/\text{cm}^2$) in the mossy cell model were increased compared with the somatic conductance and capacitance (Table 2) to account for the surface area contribution of spines.

In some simulations, the “nonspontaneously active” mossy cell model described in the preceding text was modified to simulate “spontaneously active” mossy cells with background synaptic activity and spontaneous firing observed in experiments (Ishizuka and Kosaka 1998; Ratzliff et al. 2004). The lower input resistance observed in

TABLE 1. Structure of model cells

Dimensions	Granule Cell	Mossy Cell	Basket Cell	HIPP Cell
Soma				
Diameter, μm	16.8	20	15	10
Length, μm	16.8	20	20	20
Number of dendrites	2	4	4 (2 apical and 2 basal)	4 (2 short and 2 long)
Number of compartments in each dendrite	4	4	4	3
Total number of compartments (Soma + dendritic compartments)	9	17	17	13
Dendritic compartments and dimensions			Apical dendrites:	Short dendrites:
Diameter \times length, μm	Dendrite in the granule cell layer: 3×50	Prox. dendrite: 5.78×50	Prox. dendrite: 4×75	Prox. dendrite: 3×50
	Prox. dendrite: 3×150	Mid 1 dendrite: 4×50	Mid 1 dendrite: 3×75	Mid dendrite: 2×50
	Mid dendrite: 3×150	Mid 2 dendrite: 25×50	Mid 2 dendrite: 2×75	Distal dendrite: 1×50
	Distal dendrite: 3×150	Distal dendrite: 1×50	Distal dendrite: 1×75	
			Basal dendrites:	Long dendrites:
			Prox. dendrite: 4×50	Prox. dendrite: 3×75
			Mid 1 dendrite: 3×50	Mid dendrite: 2×75
			Mid 2 dendrite: 2×50	Distal dendrite: 1×75
			Distal dendrite: 1×50	
References	Aradi and Holmes (1999)	Based on morphological data in Buckmaster et al. (1993)	Based on morphological data in Bartos et al. (2001); Geiger et al. (1997)	Based on morphological data in Buckmaster et al. (2002a); Freund and Buzsaki (1996)

HIPP, hilar perforant-path associated cell.

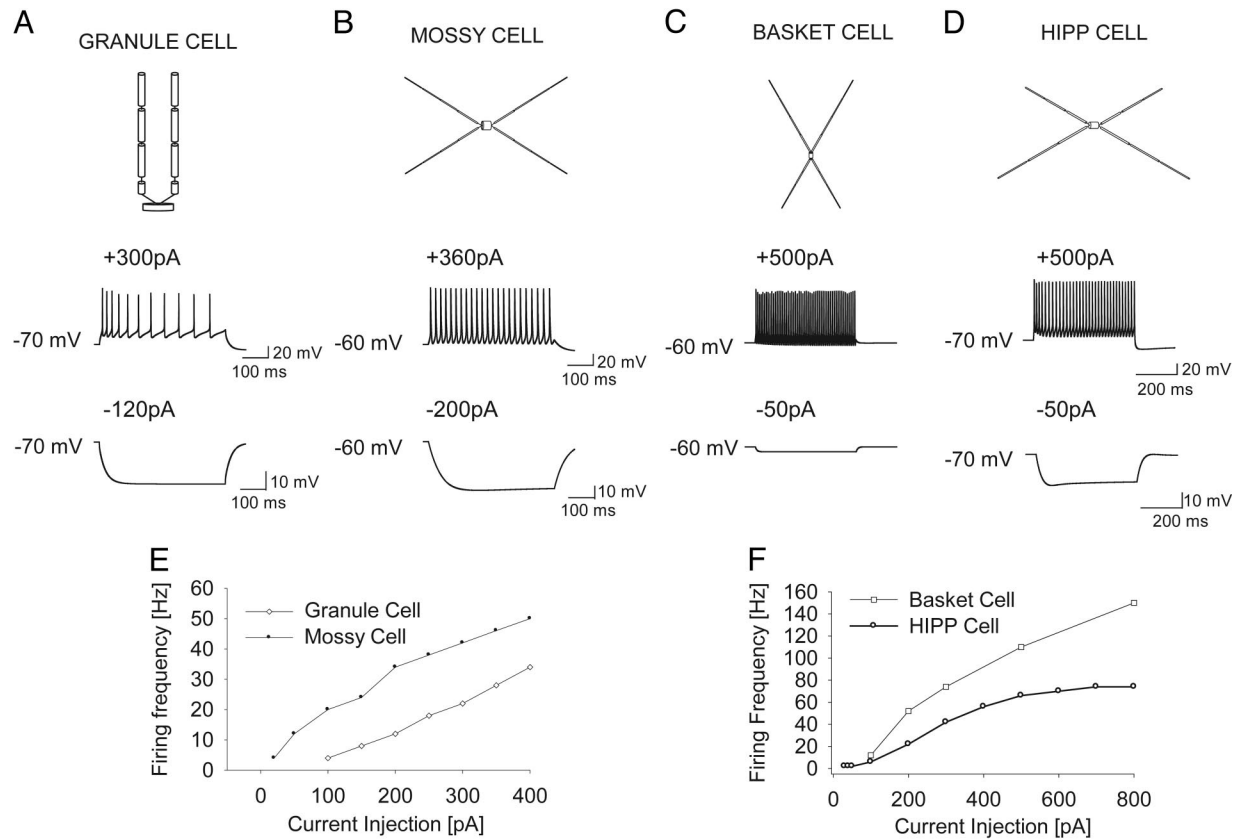


FIG. 1. Structure and intrinsic excitability of model cells. *A*: schematic representation of the structure (*top*) of the granule cell model and membrane voltage traces of the granule cell in response to +300-pA (*middle*) and -120-pA (*bottom*) current injections. *B*: illustration of the structure of the model mossy cell (*top*) and the membrane voltage responses to +360-pA (*middle*) and -200-pA (*bottom*) current injections. *C*: the structure of the model basket cell (*top*) and responses to +500 pA (*middle*) and -50 pA (*bottom*) current injections. *D*: structure (*top*) and responses to +500 pA (*middle*) and -50 pA (*bottom*) of the model hilar perforant-patch associated cells (HIPP cells). *E* and *F*: firing rates of the model granule and mossy cells (*E*) and basket and HIPP cells (*F*) in response to increasing current injection.

mossy cells in the presence of background synaptic activity (Ratzliff et al. 2004), compared with the input resistance in ionotropic glutamate and GABA receptor antagonists (Lubke et al. 1998), was simulated by including a simplified model background synaptic activity in the spontaneously active mossy cells. The synaptic background activity was simulated as a fluctuating point conductance with balanced excitation and inhibition, adapted from Destexhe et al. (2001). The background excitatory synaptic activity had a conductance of 0.012 ± 0.003 (SD) μS and a 2.7-ms time constant and reversed at 0 mV. The background inhibitory synaptic activity had a

$0.0573 \pm 0.0066 \mu\text{S}$ conductance and a time constant of 10.4 ms and reversed at -70 mV. In addition to the elevated conductance, a constant current injection ($I_{\text{depol}} = 0.65 \text{ nA}$) was included in the spontaneously active mossy cell to simulate the 2- to 4-Hz spontaneous firing rate of biological mossy cells (Ishizuka and Kosaka 1998; Ratzliff et al. 2004).

As detailed in Table 3, the intrinsic properties of model cells illustrated in Fig. 1 are consistent with the data from biological counterparts in ionotropic receptor blockers. In agreement with experimental data (Lubke et al. 1998), input resistance of the model

TABLE 2. Passive parameters and maximum conductance of the channels in model cell somata

Mechanism	Source	Granule Cell	Mossy Cell	Basket Cell	HIPP Cell
C_m , $\mu\text{F}/\text{cm}^2$		1	0.6	1.4	1.1
R_a , Ωcm		210	100	100	100
Leak conductance [S/cm^2]	Aradi and Holmes (1999)	0.00004	0.000011	0.00018	0.000036
Sodium [S/cm^2]	Aradi and Soltesz, (2002)	0.12	0.12	0.12	0.2
Delayed Rectifier K (Slow) [S/cm^2]	Aradi and Holmes, (1999)	0.006	X	X	X
Delayed Rectifier K (Fast) [S/cm^2]	Aradi and Soltesz, (2002)	0.016	0.0005	0.013	0.006
A-Type K [S/cm^2]	Aradi and Soltesz, (2002)	0.012	0.00001	0.00015	0.0008
I_h [S/cm^2]	Chen et al 2001	X	0.000005	X	0.000015
L-Type Calcium [S/cm^2]	Migliore et al. 1995	0.005	0.0006	0.005	0.0015
N-Type Calcium [S/cm^2]	Aradi and Holmes, 1999	0.002	0.00008	0.0008	X
T-Type Calcium [S/cm^2]	Aradi and Holmes, 1999	0.000037	X	X	X
Ca-dependent K (SK) [S/cm^2]	Aradi and Holmes, 1999	0.001	0.016	0.000002	0.003
Ca and Voltage-dependent K (BK) [S/cm^2]	Migliore et al. 1995	0.0006	0.0165	0.0002	0.003
Time constant for decay of intracellular Ca [ms]	Aradi and Soltesz, 2002	10	10	10	10
Steady-state intracellular Ca concentration [mol]	Aradi and Soltesz, 2002	5×10^{-6}	5×10^{-6}	5×10^{-6}	5×10^{-6}

TABLE 3. *Physiological properties of individual cell types*

Physiological Property	Granule Cell		Mossy Cell		Basket Cell		HIPP Cell	
	Model	Biological	Model	Biological	Model	Biological	Model	Biological
RMP, mV	-70.4	-75 ± 2	-60	-59.7 ± 4.9	-60	-56 to -66	-70	-65 ± 6
R _{in} [MΩ]	183	107 to 228	210	199 ± 19	64.7	56 ± 9	350	371 ± 47
τ _{memb} [ms]	30	31 ± 2	54	24 to 52	8	9-11	17.6	16.9 ± 1.8
AP amp. [mV]	80	86.6 ± 0.7	88	89.8 ± 1.1	78	74 mV	90	83
AP threshold [mV]	-48.70	-49 ± 0.8	-52	-47.33 ± 1.45	-49	-40.5 ± 2.5 (< -52)	-50	-50
Fast AHP [mV]	-7.91	-22.5 to -3.4	-12.2	-15.5	-23.39	-24.9 to -14.9	-18.5	-20 to -7
Spike frequency adaptation	0.31	0.3	0.86	0.8	0.97	.98	0.8	0.82 ± 0.42
Sag ratio	1	0.97 ± 0.01	0.97	0.81 ± 0.02	1	0.9 to 1	0.83	0.78-0.86
Source of biological cell parameters	Lubke et al. (1998); Santhakumar et al. (2000); Staley et al. (1992)		Lubke et al. 1998; Ratzliff et al. 2004; & Santhakumar et al. 2000		Bartos et al. 2001; Geiger et al. 1997; Harney and Jones, 2002; Lubke et al. 1998 & Mott et al. 1997		Lubke et al. 1998 & Mott et al. 1997	

Amplitude of the fast afterhyperpolarization (fast AHP), spike-frequency-adaptation ratio, and sag ratio were calculated as detailed in Lubke et al. (1998). Values are means ± SD.

basket cell is lower than in the HIPP cell (Fig. 1, C and D, bottom, and Table 3).

Modeling synaptic conductances

Because previous experimental studies have demonstrated the presence of posttraumatic hyperexcitability in *N*-methyl-D-aspartate

(NMDA) blockers (Santhakumar et al. 2000), only AMPA and fast GABAergic synapses were included in the networks. Postsynaptic conductances were represented as a sum of two exponentials (Bartos et al. 2001). The peak conductance (g_{max}), rise and decay time constants, and the delay of the various network connections listed in Table 4 were estimated from experimental data (Bartos et al. 2001; Geiger et al. 1997; Kneisler and Dingledine 1995a; Santhakumar et al.

TABLE 4. *Synaptic parameters of dentate network*

From (column)/ To (row)	Granule Cell	Mossy Cell	Basket Cell	HIPP Cell
AMPA				
Perforant path				
G_{max} nS	20	5	10	X
Rise ms	1.5	1.5	2	X
Decay ms	5.5	5.5	6.3	X
Delay ms	3	3	3	X
Location	Distal dendrite	Distal dendrite of 2/15 cells*	Distal dendrite	X
Granule cell				
G_{max} nS	2 (or 0.5)	0.2 (or 0.7)†	4.7	0.5
Rise ms	1.5	0.5	0.3	0.3
Decay ms	5.5	6.2	0.6	0.6
Delay ms	0.8	1.5	0.8	1.5
Location	Prox. dendrite	Prox. dendrite	Prox. dendrite	Prox. dendrite
Mossy cell				
G_{max} nS	0.3	0.5	0.3	0.2
Rise ms	1.5	0.45	0.9	0.9
Decay ms	5.5	2.2	3.6	3.6
Delay ms	3	2	3	3
Location	Prox. dendrite	Prox. dendrite	Prox. apical dendrite	Mid dendrite
GABA_A				
Basket cell				
G_{max} nS	1.6	1.5	7.6	X
Rise ms	0.26	0.3	0.16	X
Decay ms	5.5	3.3	1.8	X
Delay ms	0.85	1.5	0.8	X
Location	Soma	Prox. dendrite	Prox. apical dendrite	X
HIPP cell				
G_{max} nS	0.5	1	0.5	X
Rise ms	0.5	0.5	0.4	X
Decay ms	6	6	5.8	X
Delay ms	1.6	1	1.6	X
Location	Distal dendrite	Mid dendrite	Distal apical dendrite	X

The maximum conductance at the synapse is G_{max} . Rise and decay time constants and the average synaptic delay, including the synaptic and average conduction delay, of the synaptic contacts are listed. AMPA reversal potential was 0 mV and E_{rev} for GABA_A was -70 mV. The placement of the synapses to somatic and dendritic compartments was based on data from Acsady et al. (1998a); Geiger et al. (1997); Buckmaster et al. (1996); Wenzel et al. (1997); Scharfman (1995); and Bartos et al. (2001). *One distal dendrite of 2 randomly selected mossy cells received perforant path input. † $G_{max} = 0.7$ nS in the presence of fluctuating baseline conductance.

2000; M. Capogna and M. V. Jones, personal communication). Note that unless specifically indicated, the delay included both the synaptic delay and the average axonal conduction delay. In some simulations, an additional axonal conduction delay, depending on the distance between the location of the pre- and postsynaptic cells, was included. The axonal conduction was assumed to be 0.25 m/s (Bartos et al. 2001). In the absence of data from the dentate hilus, experimental data from CA3 was used to constrain the parameters of synapses between mossy cells and interneurons (Aaron and Dichter 2001; Kneisler and Dingledine 1995b; Lawrence et al. 2004). Kinetic data from experiments performed at room temperature were modified to physiological temperature using a Q_{10} estimate of 3 (Collingridge et al. 1984). The axons were modeled implicitly, and when the membrane potential of the presynaptic cell crossed a preset threshold, the target synapse was activated after a period equivalent to the delay (Bartos et al. 2001). The perforant-path stimulation of the dentate network was modeled as a single presynaptic stimulus from an artificial source.

Network models

The dentate network was simulated with 500 granule cells (*cells 0–499*), 15 mossy cells (*cells 506–520*), 6 basket cells (*cells 500–505*), and 6 HIPP cells (*cells 521–526*). In general, two types of networks were constructed, nontopographic and topographic. In the nontopographic network, the postsynaptic targets of each cell in the network were selected at random from the pool of potential target neurons while maintaining the cell type specific divergence and convergence. The axonal divergence of each cell type estimated from biological dentate gyrus was scaled down in the model network. The nontopographic network was not constrained by the axonal arborization pattern of the individual cell types (e.g., the spatial distribution of a single mossy fiber in the biological hippocampus is restricted to a single hippocampal lamella). The topographic network, on the other hand, was designed to incorporate the axon distribution of the cell types (both excitatory and inhibitory cells; see Table 5), in addition to the estimated divergence and convergence.

Construction of topographic networks

GENERAL STRATEGY. Organization of the topographic network was simulated by distributing the neurons in a ring structure, adapted to avoid edge effects in reduced network simulation (Wang et al. 2004). Control simulations with linear topographic strip networks were also performed (Fig. 3, C–E). Each cell type, including the granule, mossy, basket, and the HIPP cells, was evenly distributed along the ring (note that no explicit ring structure was used in the nontopographic network because, given the nontopographic random distribution of the connections, there was no real difference between the positions of the cells and thus there were no edge effects). The general procedure used to assign synaptic contacts in the topographic networks is described in the following text. Figure 2A illustrates a schematic of the connections included in the network. A schematic of the topographic pattern of connectivity is shown in Fig. 2B. The cell type specific details of the number and spatial distribution of connections are listed in Table 5.

For each synaptic connection, first, the acceptable spatial range of postsynaptic target cells was determined based on the axonal distribution pattern of the presynaptic cell described in the literature. Note that this was the only step that was implemented exclusively in the topographic network and not the nontopographic network construction. Second, the postsynaptic cells were selected at random from the pool of potential targets with uniform probability. Target synapses were placed in the compartment corresponding to the location of synaptic contacts in filled and reconstructed axons (Table 4) (Acsady et al. 1998b; Buckmaster et al. 1996; Geiger et al. 1997; Sik et al. 1997). Third, to avoid the possibility that some cells in the network receive a large number of synapses while other cells are disconnected from the network, we included a constraint on the maximum convergence of synapses on the prospective postsynaptic target from a presynaptic cell (source) class. The average convergence on a postsynaptic target cell ($Di*Pr/Po$) was calculated from the presynaptic axonal divergence (Di) and the numbers of presynaptic (Pr) and postsynaptic cells (Po). The maximum convergence was the lowest integer that was 10% more than the average convergence. While the randomized selection of postsynaptic targets provided an opportunity for variability in the synaptic convergence from a presynaptic cell

TABLE 5. Network parameters

From (column)/To (row)	Granule Cell	Mossy Cell	Basket Cell	HIPP Cell	References
Granule cell					
Divergence	Sprouted	1:1	1:1	1:3	Acsady et al. (1998); Buckmaster and Dudek (1997)
Topographic postsynaptic target pool	100 local cells	3 local cells	3 local cells	5 local cells	
Convergence [mean \pm SD] synapses/postsynaptic cell	Varied with sprouting	33 \pm 0.09	83.33 \pm 2.26	250 \pm 6.7	
Mossy cell					
Divergence	1:200	1:3	1:1	1:2	Buckmaster et al. (1996); Wenzel et al. (1997)
Topographic postsynaptic target pool	350 cells excluding the central 50 cells	6 local cells	3 cells excluding the middle cell	5 local cells	
Calculated convergence	6.0 \pm 0.05	3.0 \pm 0.3	2.5 \pm 0.5	5.0 \pm 0.5	
Basket cell					
Divergence	1:100	1:3	1:2	X	Sik et al. (1997)
Topographic postsynaptic target pool	140 local cells	7 local cells	3 local cells	X	
Calculated convergence	1.2 \pm 0.03	1.2 \pm 0.24	2 \pm 0.36	X	
HIPP cell					
Divergence	1:160	1:4	1:4	X	Buckmaster et al. (2002); Sik et al. (1997)
Topographic postsynaptic target pool	260 local cells	5 local cells	5 local cells	X	
Calculated convergence	1.92 \pm 0.03	1.6 \pm 0.16	4.0 \pm 0.45	X	
Total synaptic input					
Before, sprouting, nS	24.68 nS				
After 10%, sprouting, nS	44.68 nS				

Divergence indicates the number of post synaptic cells (in the title row) that a presynaptic cell (in the "from" column) contacts. Local cells refer to the spatially proximal cells in the ring structure. Values are means \pm SD.

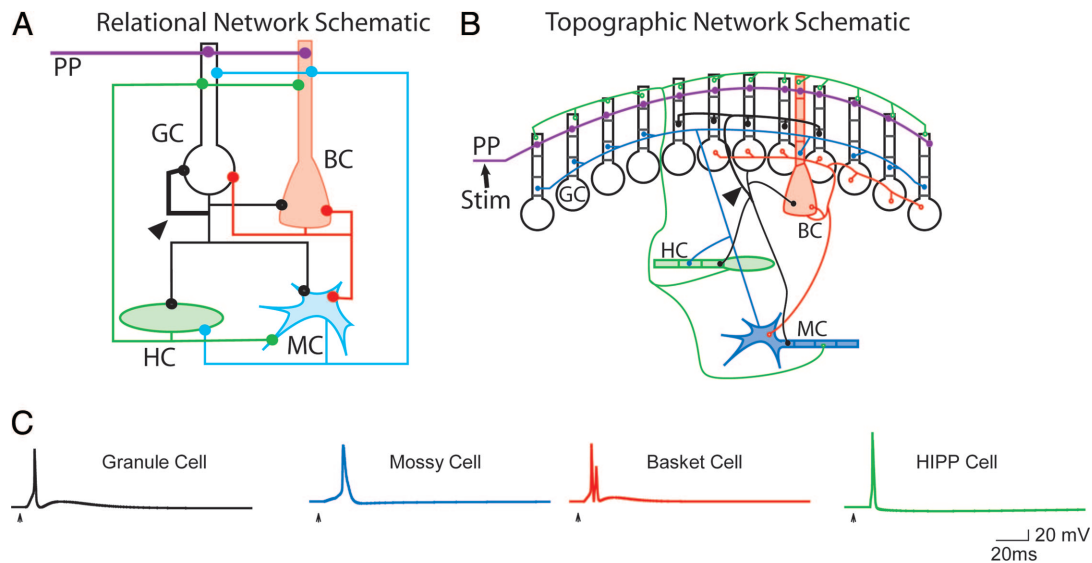


FIG. 2. Basic circuitry and synaptic responses of the cell types. *A*: a relational schematic representation of the network connections among granule cells, mossy cells, basket cells, and HIPP cells. \blacktriangle , the sprouted mossy fiber (in bold). The perforant-path input to the granule and basket cells is also illustrated. *B*: schematic of the topographic network connections between the cell types illustrates the location of the synapses and the distribution of the axon terminals. In agreement with the lamellar distribution of mossy fibers, the postsynaptic target of the granule cell axons were located on spatially proximal cells. Similarly, basket cell axons contacted nearby granule, basket, and mossy cells. Mossy cell axons conformed to the bimodal axonal distribution pattern (see METHODS) and contacted granule and basket cells on either side of the lamella in which their somata was located. HIPP cell axons contacted granule, basket, and mossy cells. The actual number and distribution of the network connections are listed in Table 5. Perforant-path synapses were located on the distal dendrites of all granule and basket cells, and the network activity was initiated by a single synchronous activation (Stim) of the perforant-path input to cells in 1 model lamella. *C*: example traces of the perforant-path-evoked responses in the model cells (note that the mossy cell in this example received a direct perforant-path input). \blacktriangle , time of stimulation. GC, granule cell; BC, basket cell; HC, HIPP cell; and MC, mossy cell.

class on the postsynaptic cells, the presence of a constraint on the maximum convergence curtailed the variability of the convergence. Finally, the presynaptic sources were connected to the appropriate target synapses and distributed randomly among the possible target dendritic branches. All synaptic connections, including the convergence of each cell from all presynaptic cell types, were written to file, to subsequently rule out the presence of disconnected cells and confirm the convergence values.

EXCITATORY AND INHIBITORY SYNAPTIC CONNECTIONS. The number of synaptic connections and axonal distribution patterns of the various cells in the network are listed in Table 5. Synapses from granule cells to mossy cells conformed to the lamellar distribution of mossy fibers (Acscady et al. 1998a; Buckmaster and Dudek 1997). Note that in the biological situation, a hippocampal lamella is defined by the septo-temporal extent of the mossy fibers (600 μm) (Buckmaster and Dudek 1997); similarly, a model lamella in this paper is also defined by the default spatial extent of the mossy fibers, encompassing 100 granule cells. Experimental data from mossy cells filled in vivo have shown that mossy cell axons have a low probability of forming synapses with granule cells located in the same lamella as their cell body, and they preferentially contact granule cells in adjacent lamellae (Buckmaster et al. 1996). To conform to this bimodal axonal arborization pattern, mossy cell axons in the topographic network synapsed on 200 of the 350 nearest granule cells, excluding the 50 granule cells located closest to the mossy cell body. Similarly (as listed in Table 5), mossy cell axonal projections to basket cells were also constrained by the bimodal distribution pattern.

PERFORANT-PATH STIMULATION. Perforant-path AMPA synapses were located on both dendrites of all granule cells and the apical dendrites of all basket cells. Because 15% of mossy cells have been shown to receive direct perforant-path input (Buckmaster et al. 1992; Scharfman 1991), we included direct perforant-path input to two randomly selected mossy cells. Perforant-path stimulation was modeled to reproduce the maximal peak AMPA conductance in response to stimulation of the perforant path in Santhakumar et al. (2000)

($G_{\text{PPtoGC}} = 40 \text{ nS}$). During focal dentate stimulation, 100 adjacent granule cells, representing a model hippocampal "lamella," were simultaneously activated by a single stimulus. Perforant-path synapses on two adjacent basket cells ($G_{\text{PPtoBC}} = 20 \text{ nS}$), and on the mossy cells with direct perforant-path input ($G_{\text{PPtoMC}} = 5 \text{ nS}$), situated in the stimulated lamella, were also activated simultaneously (the 40-nS AMPA conductance used for granule cells was decreased for basket cells and mossy cells to conform to the lower estimates of perforant-path input convergence on these cell types) (Patton and McNaughton 1995). In all the network simulations in Figs. 2–7, network activity was initiated by a single discrete (0.1 ms), synchronous activation of the perforant-path synaptic input to postsynaptic cells in a single lamella. Note that there was no additional current injection to the granule cells, nonspontaneously active mossy cells, basket cells and HIPP cells for the entire duration of the simulation.

Comparison of the evoked responses of model and biological dentate neurons

Stimulation of the perforant-path input evoked a single action potential in the directly stimulated granule cells in the normal (non-sprouted) dentate network with intact inhibition (Fig. 2C) in agreement with the recordings from granule cells in vitro (Fricke and Prince 1984; Santhakumar et al. 2000). The stimulation paradigm also evoked monosynaptic excitatory postsynaptic potentials (EPSPs) resulting in a single action potential in the directly activated mossy cells (Fig. 2C), and polysynaptic EPSPs with or without firing in mossy cells postsynaptic to the stimulated granule cells. The mossy cell response is consistent with experimental data demonstrating EPSPs or single action potentials in mossy cells after perforant-path stimulation recorded in NMDA receptor antagonists (Scharfman 1993). Similar to biological interneurons (Buckmaster et al. 2002a), dentate input activation evoked a long latency action potential in HIPP cells, in contrast to the short latency burst firing in basket cells (Fig. 2C). These simulations demonstrated that the model network was able to repro-

duce the normal (control) behavior of the various cell types in the dentate gyrus.

Simulating mossy fiber sprouting and mossy cell loss

Mossy fiber sprouting was modeled by adding synaptic connections from granule cells to the proximal dendrites of granule cells. Experimental data from filled and reconstructed granule cells in the pilocarpine model of seizures, a model system with a particularly high density of mossy fiber sprouting (Nadler 2003), indicate that 80–90% of the granule cells sprout ~500 new synapses in the inner molecular layer of the dentate gyrus (Buckmaster et al. 2002b). Therefore each granule cell would be expected to receive ~400 new synaptic inputs. The peak conductance of the unitary sprouted synapse was assumed to be 0.5 nS, consistent with the values estimated from unitary mossy fiber EPSCs in granule cells in the pilocarpine model of seizures (Molnar and Nadler 1999). Hence, we estimated that the 400 new synapses with 0.5-nS peak conductance each would result in a maximum sprouted synaptic input of 200 nS (g_{\max}) in granule cells. Because adding 400 sprouted synapses would have resulted in an unrealistically highly interconnected network, we assumed that 100 new sprouted synapses represented 100% mossy fiber sprouting in our scaled down network. Additionally, our assumption of a maximum of 100 sprouted synapses made it possible to distribute the sprouted axonal contacts within our model lamella of 100 granule cells. To conserve the maximum conductance due to sprouting in the granule cell, we divided the 200-nS maximum conductance (estimated as described in the preceding text) among 100 granule cell recurrent connections. Consequently, the conductance of a single sprouted synapse was 2 nS, and the number of sprouted synapses numerically represented the percent mossy fiber sprouting. The density of mossy fiber sprouting examined in this study was restricted to 0–50% to simulate the mild to moderate increase in mossy fiber sprouting after concussive head injury (Santhakumar et al. 2001). Note that 100% sprouting represents the degree of sprouting observed after pilocarpine induced seizures (Buckmaster et al. 2002b). Consistent with the tight, intra-lamellar distribution of sprouted mossy fibers in vivo (Buckmaster et al. 2002b), sprouted synapses from each granule cell were spatially distributed among 100 neighboring granule cells (50 on either side) in the topographic model. Autaptic connections on granule cells were not excluded.

Some control simulations incorporated a sprouted synaptic conductance of 0.5 nS with four times the convergence of mossy fiber to granule cell synapses (e.g., with 10% sprouting, each granule cell received inputs from 40 neighboring granule cells instead of 10). These control simulations were performed to verify that the increased unitary conductance of the sprouted synapse (from 0.5 to 2 nS) assumed in this study did not alter the overall network behavior. In additional simulations, the spatial spread of sprouted synapses was systematically increased to examine the effect of the topography of mossy fiber sprouting on the spread of network excitability. The topographic constraints on sprouted synapses were not imposed in the nontopographic network.

Complete mossy cell loss was simulated by removing all synaptic contacts to and from mossy cells. For 50% mossy cell loss, eight randomly selected mossy cells were “killed” by eliminating all synapses to and from the “dead” cells.

Data analysis

The activity of the network in response to focal activation of the perforant-path input was visualized in the form of spike time rasters. The activity of granule cells is presented as the mean \pm SE of the number of spikes averaged over the 500 cells during the period of simulation. The population coherence was calculated as described previously (Foldy et al. 2004; White et al. 1998). Briefly, for a pair of discharging neurons, trains of square pulses were generated for each

of the cells with each pulse of height unity being centered at the spike peak and the width being 20% of the mean firing period (interspike interval) of the faster cell in the pair. Next, the cross-correlation was calculated at zero time lag of these pulse trains, which is equivalent to calculating the shared area of the unit height pulses. Coherence was defined as the sum of the shared areas divided by the square root of the product of the total areas of each individual train (Foldy et al. 2004; White et al. 1998). The average coherence was calculated from the coherence values obtained for all cell pair combinations.

RESULTS

Increase in dentate excitability with mossy fiber sprouting

NONTOPOGRAPHIC DISINHIBITED NETWORK. First, we examined the effect of mossy fiber sprouting on the dentate excitatory network by setting all inhibitory synaptic conductances in the network to zero (“disinhibited” network). As a first step, we focused on granule cell firing in the disinhibited, normal (0% sprouting), nontopographic network (constrained only by the cell-type-specific axonal divergence). Consistent with the experimental data (Fricke and Prince 1984; Santhakumar et al. 2000) and earlier simulation studies (Lytton et al. 1998), stimulation of perforant-path inputs in our model evoked only a single action potential in the monosynaptically activated granule cells, even though the network had no GABAergic inhibition (Fig. 3A1). Note that only the *granule cells 0–99* (plotted on the y axis in Fig. 3A1) received direct stimulation, and only these cells fired a single action potential, whereas all the other granule cells remained quiescent.

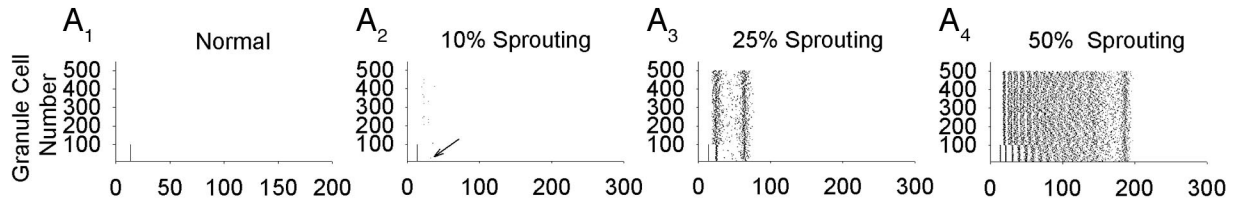
Next, the degree of recurrent mossy fiber sprouting was systematically increased from 0 to 50%. Even 10% sprouting (representing the addition of 10 recurrent mossy fiber contacts per granule cell; see METHODS) caused the activity to spread from the directly activated granule cells to the others (*granule cells 100–499* in Fig. 3A2). Additionally, some of the directly stimulated granule cells responded with more than one action potential (Fig. 3A2, \leftarrow), further indicating the greater excitability of the network with 10% sprouting compared with the normal network (Fig. 3A1). Increasing mossy fiber sprouting to 25 and 50% resulted in a more robust spread of the activity, including the activation of all granule cells in the network and prolongation of the duration of the stimulation-triggered network activity (Fig. 3A, 3 and 4). Importantly, however, the network activity was self limiting and failed to progress beyond 200 ms even in networks with 50% mossy fiber sprouting (Fig. 3, A4 and D). It is likely that the characteristically hyperpolarized resting membrane potential and strong adaptation of granule cells limited their excitability (Lytton et al. 1998), even in the absence of feed-back inhibitory circuits.

TOPOGRAPHIC DISINHIBITED NETWORK. Next, we examined the effect of sprouting in the topographic (and disinhibited) network (Fig. 3B, 1–4). When the topographic constraints were included, focal excitation of 100 granule cells in the absence of sprouting still resulted in a single action potential only in the monosynaptically activated granule cells (Figs. 3, B1 and C1, and 4A1). In contrast to the nontopographic network, however, even the low (10%) sprouting in the topographic ring network resulted in the spread of the activity to all granule cells (Fig. 3B2; note that the arrowhead-like shape of the raster plot originates from the fact that *cells 0–99* were activated first, and, because of the ring structure of the network, *cells 0* and

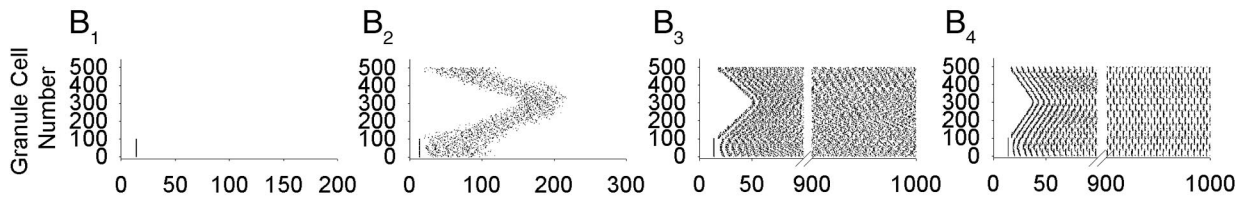
499 are neighbors). The spread of granule cell activity in the linear topographic strip network (Fig. 3C, 1 and 2) in which a single lamella in the middle of the strip (*cells 200–299*) was activated was similar to the topographic ring network. In addition to the extra-lamellar spread of the activity with 10%

sprouting in the topographic networks, the average granule cell firing was also higher compared with that in the nontopographic network (Fig. 3D, *inset*). With increased levels of mossy fiber sprouting, the activity spread faster throughout the network, and it became self-sustaining (i.e., lasting at least as

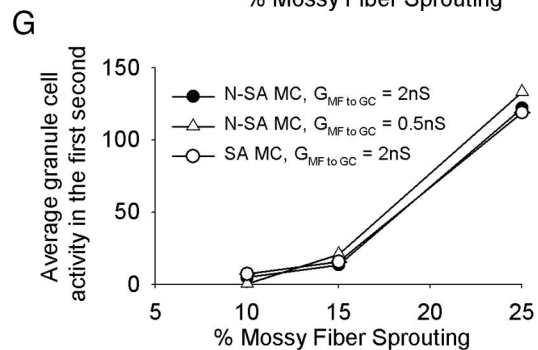
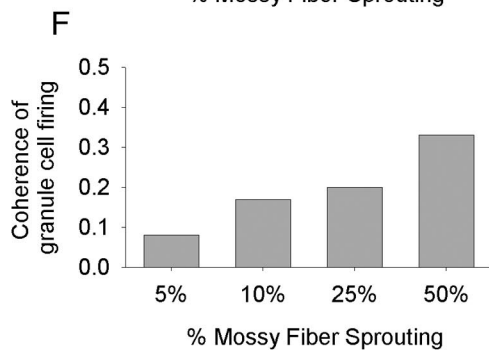
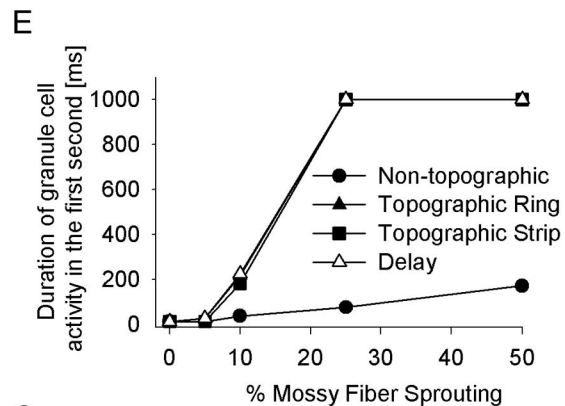
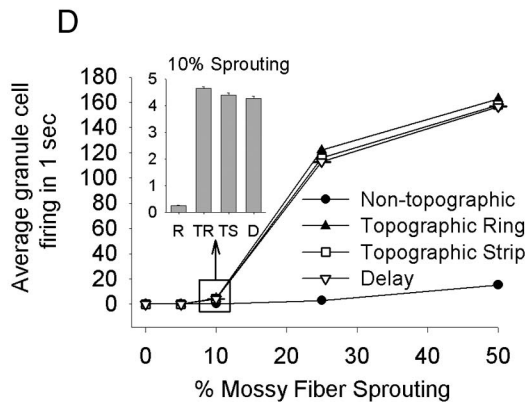
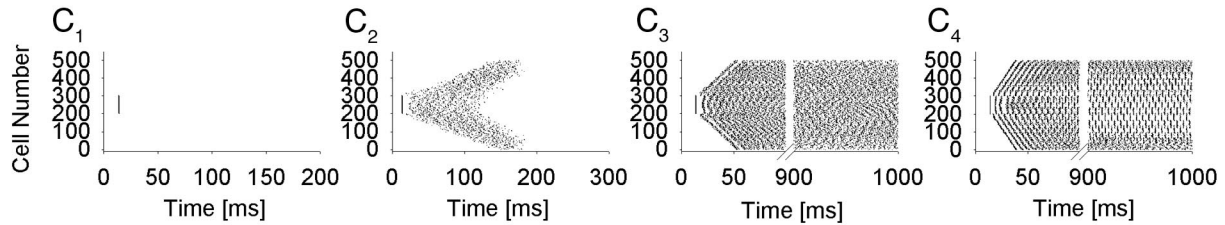
Granule cell spike rasters in non-topographic disinhibited networks



Granule cell spike rasters in topographic ring disinhibited networks



Granule cell spike rasters in topographic strip disinhibited networks



long as the duration of the simulation, which was 5 s; note that only the 1st second is plotted in the figures; Fig. 3*B*, 3 and 4, and *C*, 3 and 4). In addition to the increase in the number of action potentials (Fig. 3*D*) and duration of granule cell activity (Fig. 3*E*) with mossy fiber sprouting in the topographic compared with the nontopographic networks, the simulations also showed enhanced coherence of granule cell firing (for calculation of coherence, see METHODS) in the topographic ring network with increasing sprouting (Fig. 3*F*) (note that the increased coherence can also be observed in the raster plots in Fig. 3*B*, 2–4).

CONTROLS FOR MODEL SIMPLIFICATIONS. We performed several control simulations to check whether the assumptions in the model altered the network behavior. First, we examined the effect of introducing axonal conduction delay in the topographic network. The inclusion of distance-dependent delay resulted in a <10% decrease in the average granule cell firing (Fig. 3*D*) but did not abolish the sustained network activity (Fig. 3*E*).

Second, we examined the impact of some of the assumptions regarding the synaptic conductance of the sprouted mossy fibers. The mossy fiber synaptic conductance after sprouting was initially set to four times the estimated unitary synaptic conductance ($4 \times 0.5 \text{ nS} = 2 \text{ nS}$; Table 4) to reflect the total conductance estimated from sprouted connections (for further explanation, see METHODS). A series of control simulations were performed with a recurrent mossy fiber synaptic conductance of 0.5 nS but with four times the number of recurrent mossy fibers converging on each granule cell. As shown in Fig. 3*G* (plots labeled nonspontaneously active mossy cells, N-SA MC), decreasing the unitary sprouted conductance and elevating the number of sprouted synapses did not change the overall behavior of the network.

Third, we examined the effect of replacing the nonspontaneously active mossy cells with spontaneously active ones (incorporating biologically realistic fluctuating baseline conductance and spontaneous firing, see METHODS) in the topographic network. As illustrated in Fig. 3*G* (plot labeled spontaneously active mossy cells, SA MC), inclusion of spontaneously active mossy cells did not alter the overall network activity.

Fourth, a final set of control simulations showed that increasing the mossy fiber to mossy cell synaptic conductance (from 0.2 to 0.7 nS; these simulations were done with nonspontaneously active mossy cells) did not alter the average activity and the spread of granule cell firing (data not shown).

Overall, the results of these control simulations indicate that the behavior of the model dentate is fairly robust to small

changes in synaptic parameters and suggest that the assumptions in the model do not significantly compromise the network response to focal stimulation.

EFFECT ON GRANULE AND MOSSY CELL ACTIVITY. Next, we analyzed in more detail the effects of mossy fiber sprouting on cell firing in the disinhibited, topographic network. First, we examined the effect of focal, lamellar stimulation on the activity of granule and mossy cells within the stimulated lamella in the normal network (0% sprouting). As mentioned in the preceding text, stimulation of the perforant-path input to the network evoked a single action potential in granule cells (Fig. 4*A1*). Mossy cells postsynaptic to the directly stimulated granule cells also fired a single action potential in response to stimulation of the model lamella (Fig. 4*B1*). This pattern of evoked activity observed in granule and mossy cells in the model is consistent with the perforant-path-evoked action potential firing in biological granule cells (average number of spikes following a single stimulation to the perforant path: 0.61 ± 0.19) and mossy cells (0.60 ± 0.60 spikes) recorded from sham-injured (i.e., control) animals in the presence of GABA_A receptor antagonist bicuculline (i.e., in a disinhibited network) (Santhakumar et al. 2000).

Next, we systematically increased the degree of mossy fiber sprouting. There was a progressive increase in the perforant-path-evoked firing in both granule and mossy cells when mossy fiber sprouting was increased. The number of action potentials following the perforant-path stimulation in granule and mossy cells in the model networks with 10% mossy fiber sprouting (Fig. 4, *A2* and *B2*; granule cells: 4.64 ± 0.06 spikes; mossy cells: 2.93 ± 0.15 spikes) was similar to the biological dentate gyrus (granule cells: 5.93 ± 1.78 spikes; mossy cells: 3.63 ± 0.72 spikes) 1 wk after concussive head injury (Santhakumar et al. 2000). When the mossy fiber sprouting was increased to 25%, some nonspontaneously active mossy cells depolarized without firing (not shown; this effect is similar to the depolarization block reported in Bikson et al. 2003; Lytton et al. 1998), whereas others fired multiple spikes (Fig. 4*B3*), with the net result being that 25% sprouting led to more mossy cell activity on average, albeit with a larger cell to cell variability (Fig. 4*D*). Mossy fiber sprouting resulted in increased mossy cell firing in networks with spontaneously active mossy cells as well (Fig. 4, *C*, 1–3, and *D*).

Taken together, these data show that the disinhibited topographic model network can simulate the effects of perforant-path stimulation in the uninjured and injured biological dentate gyrus in bicuculline. Interestingly, the 10–15% sprouting, at which the granule cell and mossy cell firing in the model was observed to be the most similar to the data obtained from the

FIG. 3. Mossy fiber sprouting enhances excitability in the dentate excitatory network. *A*, 1–4: spike raster plots showing the activity of granule cells in the nontopographic networks in response to stimulation of the perforant-path input to the network. The degree of mossy fiber sprouting was increased from 1 to 4. ← in *A2*, the 2nd spike of a granule cell that fired more than 1 action potential in response to stimulation. *B*, 1–4: granule cell spike rasters from topographic-ring networks illustrate the spread of perforant-path-evoked activity with increasing mossy fiber sprouting. *C*, 1–4: granule cell spike rasters from control simulations from the linearized topographic-strip networks show the spread of perforant-path-evoked activity with increasing mossy fiber sprouting. *D*: summary plot showing the effect of sprouting on the average granule cell firing in the nontopographic, topographic-ring, topographic-strip, and topographic networks with axonal conduction delay (Delay). *Inset*: histogram of the average granule cell firing in networks with 10% sprouting in the boxed region in *C* in nontopographic network (NT), topographic-ring (TR) network, topographic-strip (TS) network, and topographic network with delay (*D*). *E*: summary graph shows the increase in duration of granule cell activity with higher degree of sprouting in the nontopographic, topographic-ring, topographic-strip, and topographic networks with delay (Delay). Note that the plots represent the maximum duration of activity in the 1st second of simulation. *F*: summary histogram shows that increasing the degree of mossy fiber sprouting increases the coherence of perforant-path-evoked granule cell firing in the topographic-ring network. *G*: control simulations showing the lack of effect of altering the strength of the sprouted mossy fiber synapses and the inclusion of spontaneously active mossy cells. Responses were evoked by stimulation of the perforant-path input to 100 granule cells in networks with 10, 15, and 25% mossy fiber sprouting. N-SA MC: nonspontaneously active mossy cell; SA MC: spontaneously active mossy cell.

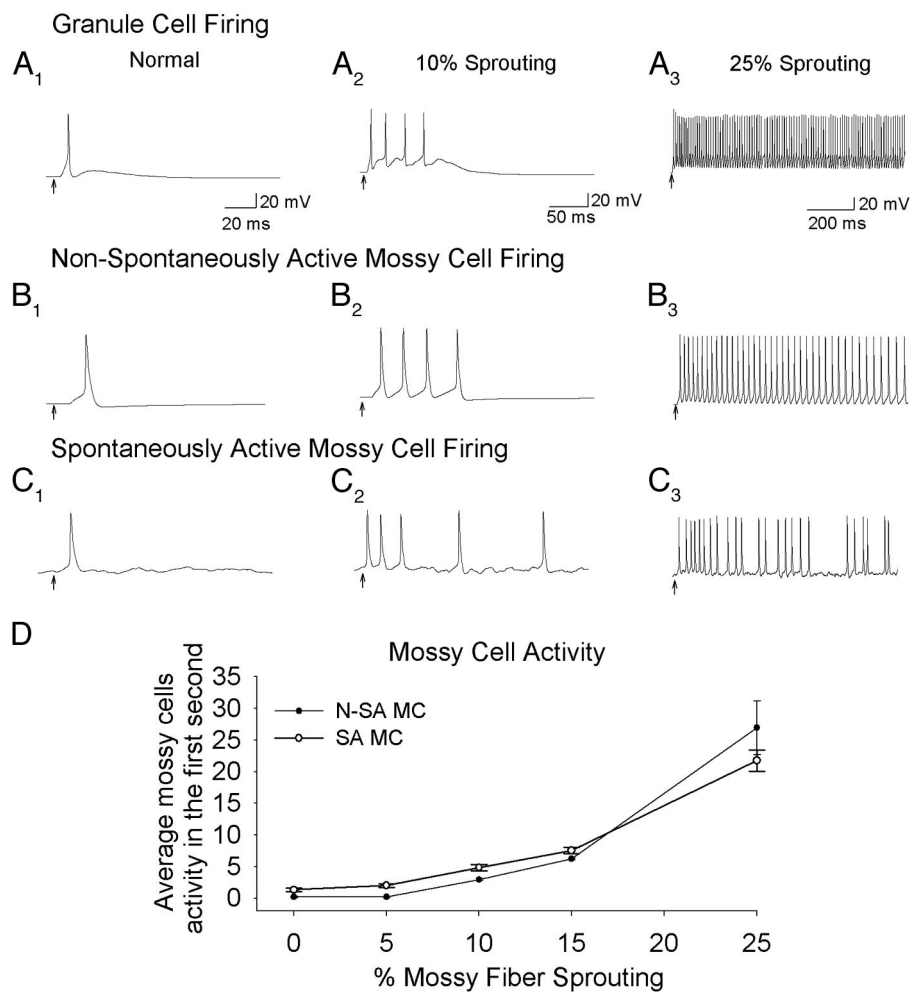


FIG. 4. Mossy fiber sprouting increases granule and mossy cell excitability in disinhibited networks. *A*, 1–3: representative membrane potential traces show the perforant-path-evoked granule cell firing in disinhibited, topographic networks. The response of a granule cell to perforant-path input in the normal network (*A*₁) and in networks with 10% (*A*₂) and 25% sprouting (*A*₃) are illustrated. *B* and *C*, 1–3: membrane voltage traces show the mossy cell response to perforant-path stimulation of networks incorporating nonspontaneously active (*B*, 1–3) and spontaneously active (*C*, 1–3) model mossy cells. *D*: summary plot of the increase in average mossy cell activity with the degree of mossy fiber sprouting in networks with N-SA MC and SA MC.

biological dentate gyrus after moderate fluid percussion head injury, matches well with the histological data indicating the presence of only relatively mild mossy fiber sprouting in the head trauma paradigm (Santhakumar et al. 2001). The results also indicate that weak mossy fiber sprouting can replicate the increase in excitability of the excitatory cell types in the dentate gyrus observed after moderate concussive head trauma even in the absence of cell loss and changes in the intrinsic properties of the cell types. Finally, comparison of the spread of perforant-path-evoked network activity in the topographic and nontopographic networks suggests that a topologically constrained network structure might aid in the generation and spread of hyperexcitability in the presence of mossy fiber sprouting.

Lamellar mossy fiber sprouting facilitates spread of focal excitation

ROLE OF SPATIAL TOPOLOGY OF SPROUTED MOSSY FIBERS. Why does the topographic network structure increase the spread of activity following focal excitation more than the nontopographic one? We hypothesized that the spatially restricted, intra-lamellar distribution of the sprouted mossy fibers (Buckmaster and Dudek 1999) is important for the induction and spread of hyperexcitability to neighboring cells.

The effect of the spatial spread of the sprouted mossy fibers on dentate excitability was investigated in topo-

graphic, disinhibited networks with 10% mossy fiber sprouting [because, as described in the preceding text, this model network appeared to best represent the experimental data obtained after head injury in the presence of bicuculline Santhakumar et al. 2001)]. Figure 5*A* illustrates granule cell spike rasters from simulations in which the spatial range of the sprouted mossy fibers was increased. In each case (i.e., in all 4 plots in Fig. 5*A*), each of the 500 sprouted mossy fibers in the network contacted 10 postsynaptic granule cells (corresponding to 10% sprouting; see METHODS), but the number (and thus the spatial range) of the granule cells from which the 10 postsynaptic granule cells were randomly chosen was systematically increased (from a pool of 50 granule cells in Fig. 5*A*₁ to 300 cells in Fig. 5*A*₄). Interestingly, as illustrated in Fig. 5*A*, the spread of activity after stimulation of the perforant-path inputs to 100 granule cells showed a maximum with increasing spatial spread of the sprouted mossy fibers. As seen in Fig. 5, *A* and *B*, the maximum occurred in the network in which the spatial spread of the sprouted mossy fiber contacts was restricted to the 100 closest granule cells (the default spatial spread of mossy fiber contacts). Inclusion of axonal conduction delays did not change the overall effects of alterations in the spatial spread of sprouted mossy fibers (Fig. 5*B*). These data suggest that the restricted, intra-lamellar topography of the sprouted mossy fibers reported in vivo (Buckmaster and

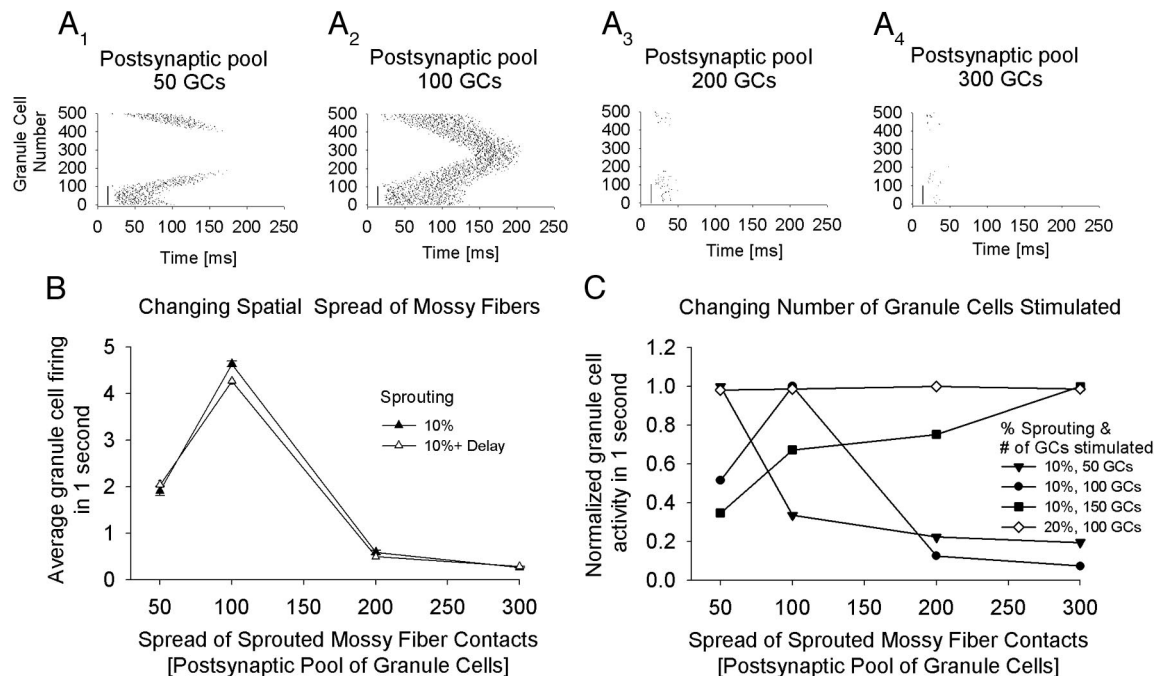


FIG. 5. Lamellar topography of sprouted mossy fiber synapses facilitates spread of focal activity. *A*, 1–4: spike raster plots showing the activity of granule cells in topographic networks with 10% sprouting with increasing spatial range of mossy fibers (measured as the pool of potential granule cells from which the 10 actually contacted cells were selected; see text for details). Responses were elicited by stimulating the perforant-path input to 100 granule cells. *B*: summary plot showing alterations in the activity of granule cells with changes in the spatial spread of sprouted mossy fiber synapses in networks with 10% sprouting with and without delay. *C*: plot of normalized granule cell firing during systematic increases in the spatial spread of the sprouted mossy fiber synapses in disinhibited networks. The number of granule cells activated by perforant-path stimulation was increased from 50 to 150 cells in the networks with 10% sprouting. The plot with open symbols presents the normalized granule cell activity in networks with 20% mossy fiber sprouting in response to stimulation of the perforant-path input to 100 granule cells. Because the maximum granule cell activity was modulated by the number of stimulated granule cells and the degree of sprouting, granule cell firing was normalized to the maximum activity in each plot. The maximum firing (average number of spikes during the 1st second after stimulation): 10%, 50 GCs: 0.51; 10%, 100 GCs: 4.61 spikes; 10%, 150 GCs: 6.76; 20%, 100 GCs: 50.00 spikes.

Dudek 1997) may play a central role in determining the spread of network activity during seizures in the dentate gyrus.

EFFECT OF THE NUMBER OF ACTIVATED GRANULE CELLS AND THE SPROUTING DENSITY. How and why does the distribution of sprouted mossy fibers modify the spread of focally evoked excitability? Although increasing the spatial spread of mossy fiber sprouting is expected to aid in the propagation of the activity beyond the initial focus, it is also likely to reduce the convergence of active inputs on neighboring granule cells and thus decrease the ability of the network to sustain firing. These two opposing factors (i.e., the broader spatial spread of the sprouted mossy fibers aiding propagation of the activity beyond the initial focus but simultaneously decreasing the convergence of the excitatory mossy fiber inputs important for sustaining the activity) are likely to underlie the existence of a maximum in Fig. 5*B*. To further examine how mossy fiber sprouting in the model network modulates the spread focal activity, we tested whether changing the number of directly activated granule cells altered the spatial spread of sprouting at which granule cell activity was maximized. When 50 neighboring granule cells were activated by the perforant-path stimulation, the maximum average network firing occurred when the spatial spread of mossy fiber sprouting was restricted to the neighboring 50 granule cells, and the activity declined progressively as the spread of mossy fiber sprouting was made wider (Fig. 5*C*, plot labeled “10%, 50 GCs”, referring to 10% sprouting). As shown earlier (Fig. 5*B*), when 100 granule cells

were activated, the network activity peaked when the sprouted terminals were distributed among 100 adjacent cells (plot “10%, 100 GCs” in Fig. 5*C*). When 150 granule cells were stimulated, the activity progressively increased as the spatial range of mossy fiber sprouting widened (plot “10%, 150 GCs”; Fig. 5*C*). When the degree of sprouting was increased to 20% (thereby increasing the possibility for convergence of active input to granule cells), alterations in the spatial spread of recurrent mossy fiber contacts had little effect on the average granule cell firing (plot “20%, 100GCs” in Fig. 5*C*).

The data in Fig. 5 indicate that a compact distribution of sprouted mossy fibers can aid in the propagation of a small focus of network activity, especially if the degree of mossy fiber sprouting is mild. If the spatial spread of sprouting is too wide, too few cells are likely to be recruited outside the initial focus to sustain the network activity (Fig. 5, *A* and *B*). Similarly, in the nontopographic network with 10% sprouting (Fig. 3*A2*), the low convergence of active input prevents the generation of sustained network activity despite the spread of the initial focus of activation to several granule cells that were not directly activated. When the number of focally stimulated granule cells is decreased (to 50 from 100 in Fig. 5*C*), mossy fiber sprouting has to be even more spatially restricted to result in maximal granule cell activity. When the number of stimulated granule cells is increased (Fig. 5*C*), a wider mossy fiber sprouting distribution becomes the most conducive to maximal granule cell firing. These findings further support the suggestion made in the preceding text that the compact lamellar

distribution of the sprouted fibers observed *in vivo* greatly aids in the initiation and spread of hyperexcitability, particularly when the mossy fiber sprouting is mild.

Mossy cell loss decreases dentate excitability

Next, we examined the effects of mossy cell loss on granule cell activity. As demonstrated earlier, focal stimulation of the perforant-path inputs to 100 granule cells resulted in a spread of the activity to the entire network in the presence of 10% sprouting and 15 nonspontaneously active mossy cells (Fig. 3B2). When axonal conduction delay was included, focal network activity under these conditions still spread to all granule cells (Fig. 6A₁). As shown by the mossy cell spike raster in Fig. 6B₁ (from the same simulation as in Fig. 6A₁), the 15 mossy cells in the network participated in the spread of activity and likely aided in the propagation of firing from the initial focus. Random deletion of eight mossy cells (i.e., ~50% of the mossy cells, close to the degree of mossy cell loss reported after moderate head trauma) (Toth et al. 1997) resulted in a decrease in the average granule cell firing and in the number of granule cells involved in the network activity (Fig. 6, A₂, C, and D). The corresponding mossy cell spike raster showed that the spread of network activity to mossy cells was also curtailed (Fig. 6B₂), presumably because the “dead” cells (■) were unable to participate in the spread of activity. Complete mossy cell loss resulted in a further decrease in the spread of activity in the network (Fig. 6A₃). However, when the degree of mossy fiber sprouting was increased to ≥15%, mossy cell loss caused little change in the average firing and

spread of network activity (Fig. 6D). Similarly, mossy cell loss reduced the network activity in simulations that included spontaneously active mossy cells and 10% sprouting, but even complete deletion of mossy cells caused only a small (<5%) decrease in network activity when sprouting was increased to 25% (Fig. 6E).

These results are in agreement with experimental data showing that deletion of mossy cells decreases granule cell activity (Ratzliff et al. 2004; Santhakumar et al. 2000). Additionally, our simulations show that mossy cell loss is less effective at decreasing excitability when the degree of mossy fiber sprouting increases, presumably because once the degree of sprouting reaches a certain level, the seizure-like activity can sustain itself and propagate through the sprouted mossy fibers even in the absence of mossy cells.

Effect of mossy fiber sprouting and mossy cell loss in networks with GABAergic inhibition

Having established the role of mossy fiber sprouting in hyperexcitability in the disinhibited network, we next examined the contribution of sprouting and mossy cell loss to perforant-path-evoked granule cell excitability in the presence of inhibitory synaptic transmission. Focal stimulation of the topographic, “normal” (i.e., without sprouting or cell loss) model dentate gyrus with inhibitory synaptic conductances caused action potential firing in the directly activated granule cells (Fig. 7A₁), local mossy cells, and interneurons (Fig. 7B₁). In the presence of 10% mossy fiber sprouting, there was an increase in the average activity of the stimulated granule cells

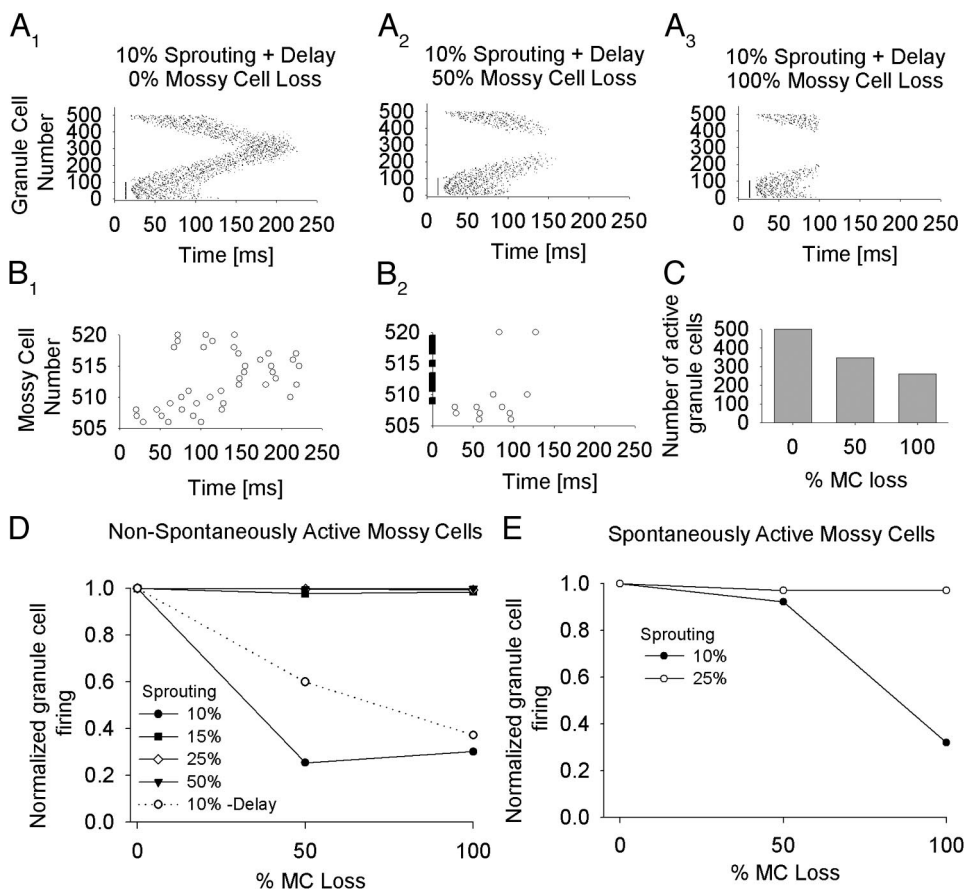


FIG. 6. Effect of mossy cell loss on dentate excitability. *A*, 1–3: granule cell spike-time raster evoked by stimulation of 100 granule cells in disinhibited dentate gyrus incorporating axonal conduction delays. Networks were simulated with 0% (*A*₁), 50% (*A*₂), and 100% (*A*₃) mossy cell loss. *B*, 1 and 2: spike-time raster plots of mossy cells in the networks illustrated in *A* with 0% (*B*₁) 50% (*B*₂) mossy cell loss. ○, spikes in mossy cells; ■, the “dead” mossy cells. *C*: summary histogram of the effect of mossy cell loss on the number of granule cells activated by stimulation of the perforant-path input to 1 model lamella in networks with 10% mossy fiber sprouting. *D* and *E*: summary plots of the granule cell activity with varying degrees of mossy cell loss and sprouting in networks with nonspontaneously active (*D*) and spontaneously active (*E*) mossy cells. Because the network activity increased with the degree of mossy fiber sprouting, the granule cell activity in each plot was normalized to the firing without mossy cell loss (average number of spikes during the 1st second after stimulation: *D*: 10% sprouting: 4.61; 15%: 13.33; 25%: 121.95; 50%: 162.81; 10% sprouting with delay: 4.27; *E*: 10%: 6.98; 25%: 118.8).

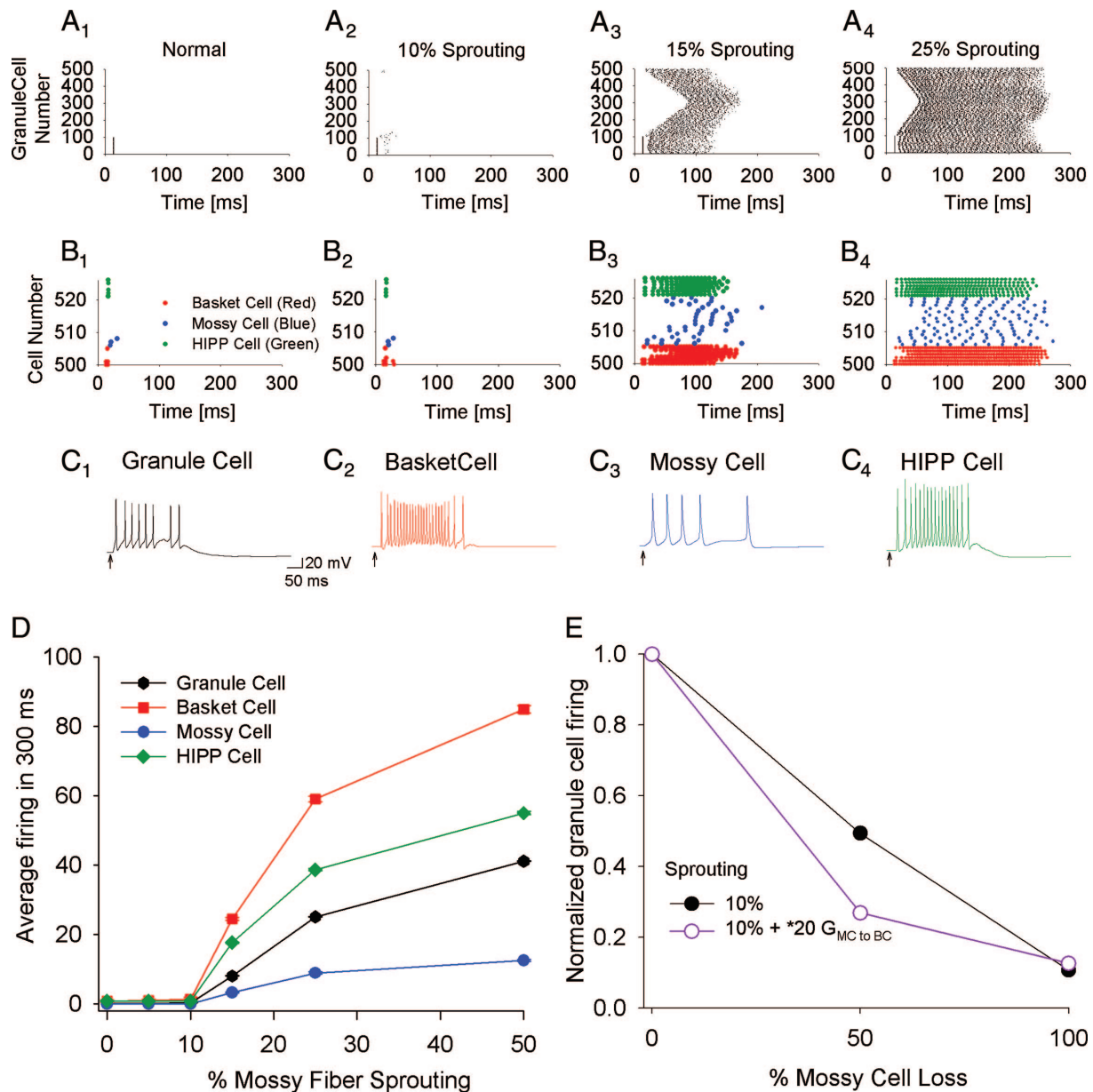


FIG. 7. Effect of sprouting and mossy cell loss on evoked activity in networks with inhibition. *A*, 1–4: raster plots illustrating the spread of activity in granule cells in the topographic dentate network with 0, 10, 15, and 25% sprouting. *B*, 1–4: spike-time raster of the activity of mossy cells (blue), basket cells (red) and HIPP cells (green) in the networks illustrated in *A*. *C*, 1–4: representative membrane potential traces from a granule cell (black), basket cell (red), mossy cell (blue), and HIPP cell (green) evoked by perforant-path stimulation in a network with 15% sprouting and intact inhibition (same simulations as in *A*3 and *B*3). *D*: summary plot showing the effect of sprouting on the average firing in the 4 cell types. *E*: effect of mossy cell loss on the perforant-path-evoked granule cell activity in networks with spontaneously active mossy cells and 10% mossy fiber sprouting. The $*20G_{MCtoBC}$ plot (in purple) represents summary data from network simulations with 20 times the mossy cell to basket cell unitary conductance. The granule cell activity was normalized to the average granule cell activity in networks without mossy cell loss (average number of spikes during the 1st second after stimulation: 10% sprouting: 2.27; 10% sprouting with $*20G_{MCtoBC}$: 1.97).

and spread of activity to cells in adjacent lamellae that were not directly stimulated (Fig. 7, *A*2 and *B*2). However, in contrast to the disinhibited network in which 10% sprouting caused the spread of focal activity to the entire network, only 18 additional granule cells were recruited in the network activity in the presence of inhibition. When the mossy fiber sprouting was increased to $\geq 15\%$, the focal activity spread to all excitatory and inhibitory cells in the network (Fig. 7, *A*, 3 and 4, and *B*, 3 and 4). Note that due to the topographic axonal distribution pattern, the activity spread progressively from the initial focus to adjacent lamellae on either side in the ring structure in all

cell types. Similar results were also obtained in the topographic strip network (data not shown). As illustrated by the membrane voltage traces from representative cells in a network with 15% sprouting (Fig. 7*C*), sprouting increased the evoked firing in all cell types in the network. Focal stimulation evoked greater activity in all cell types in the networks with higher density of mossy fiber sprouting (Fig. 7*D*). Additionally, deletion of mossy cells decreased the network activity even in the presence of inhibition (Fig. 7*E*), in agreement with experimental data (Ratzliff et al. 2004) and with the predictions of the “irritable mossy cell” hypothesis (Ratzliff et al. 2002; Santhakumar et al.

2001). However, these results contradicted the predictions of the “dormant basket cell” hypothesis (Sloviter 1991; Sloviter et al. 2003), according to which mossy cell loss should lead to a hyperexcitable response because basket cells lose their excitatory inputs from mossy cells. In an effort to maximize the mossy cell excitation of basket cells, additional simulations were also carried out where the mossy cell to basket cell synaptic conductance was increased ≤ 20 times the unitary conductance. However, even in these networks, the loss of mossy cells did not increase granule cell activity (Fig. 7E).

DISCUSSION

Concussive head injury increases the risk for temporal lobe epilepsy (TLE) by mechanisms that are not fully understood (Annegers and Coan 2000; Jennett 1975). This study focused on examining the role of two prominent histopathological features common to both TLE and head injury, mossy fiber sprouting and hilar excitatory cell loss, in modulating excitability of the dentate gyrus. A computational approach was adopted to investigate the contribution of specific levels of mossy fiber sprouting and mossy cell loss without the confounding effects of coincident changes that might occur *in vivo*. The simulation results demonstrate that 1) even a low level of mossy fiber sprouting is sufficient to cause an increase in dentate excitability in response to lamellar perforant-path activation. 2) Compact axonal distribution of the sprouted mossy fibers can aid in the spread of a small focus of hyperexcitability in networks with moderate mossy fiber sprouting. And 3) removal of mossy cells decreases granule cell excitability and impedes the propagation of network hyperexcitability, indicating that surviving mossy cells amplify dentate excitability even without changes in intrinsic or synaptic properties (Ratzliff et al. 2002).

Close correspondence between the modeling and experimental data

The present study was carried out to examine how alterations in the dentate gyrus after seizures and head injury contribute to network hyperexcitability. Earlier computational studies have investigated the role of recurrent excitatory collaterals in epileptiform activity in CA3 (Traub et al. 1987, 1994) and the neocortex (Bush et al. 1999). The role of mossy fiber sprouting in network hyperexcitability in the dentate gyrus after kindling was previously investigated in an elegant, highly reduced model of the dentate gyrus, containing 50 granule cells and 4 hilar cells (2 mossy cells and 2 interneurons), each with a somatic and dendritic compartment (Lytton et al. 1998). Lytton et al. (1998) constrained the maximal sprouted synaptic conductance using the maximum perforant-path conductance parameters (rather than the estimated sprouted synaptic conductance used in this study) and showed that 1–5% of the maximum sprouted conductance could lead to network hyperexcitability. However, as a consequence of the small size, the network was highly interconnected, which might have caused synchronous activity in the network. Additionally, because the network implemented only two mossy cells, the effect of mossy cell loss on network excitability was not investigated by Lytton et al. (1998). In this study, we expanded this earlier dentate model to be able to examine the

effect of posttraumatic mossy cell loss in addition to recurrent excitatory sprouting. Specifically, the network size was increased ~ 10 -fold to include 500 granule cells, 15 mossy cells, and 12 interneurons. Similar to Lytton et al. (1998), the network size was limited by the need to use multicompartmental models that reproduced the characteristic biophysical properties of the various cell types. Each cell type was modeled with a somatic and 8–16 dendritic compartments to allow for the spatial location of synapses to distinct apical and basal dendritic regions. Two distinct classes of interneurons, basket cells with perisomatic projections and HIPP cells targeting the distal dendrites, were also included. Importantly, our model included the axonal topography of the cell types and number of sprouted synaptic contacts based on recent experimental data.

The synaptic weights and axonal connectivity of the network were constrained by unitary synaptic conductance and axonal divergence estimated from experimental data (see METHODS). Focal stimulation of the control network closely replicated the firing patterns of the biological cell types. Additionally, the perforant-path-evoked responses of the control network was robust to changes in the state of activity of mossy cells (nonspontaneously active versus spontaneously active). Inclusion of axonal conduction delay, which has been shown to modulate network synchrony (Maex and De Schutter 2003), had relatively little effects on dentate excitability in the presence of moderate sprouting, presumably because of the relatively small physical distances present in our reduced, 527-cell network. Furthermore, similar to the results of recent experiments (Ratzliff et al. 2004), there was a decrease in granule cell excitability with mossy cell loss. Using the network model that replicated behavior of the normal dentate gyrus, we have shown that approximately a 10th of the mossy fiber sprouting observed after pilocarpine treatment (Buckmaster et al. 2002b) can reproduce the perforant-path stimulation-evoked granule and mossy cell hyperexcitability in the posttraumatic dentate gyrus (Santhakumar et al. 2000). The low degree of mossy fiber sprouting at which the postinjury dentate excitability was simulated is consistent with the mild to moderate sprouting observed within a week after concussive injury (Santhakumar et al. 2001). The larger increase in dentate excitability with higher degrees of mossy fiber sprouting is in agreement with the robust sprouting and increased incidence of spontaneous seizures with severe head injury (Golarai et al. 2001; Nissinen et al. 2003).

Simplifications adopted in the model

Several simplifications were made in modeling the individual cells and implementing the dentate network. A uniform distribution of conductances (other than for fast sodium and delayed rectifier potassium conductances) was adopted for all cell types, with the exception of granule cells, for which the channel distributions have been estimated (Aradi and Holmes 1999). Although the actual distribution of channels might be important to synaptic integration in the dendrites (Johnston et al. 1996; Magee 2000), we assumed a uniform distribution due to the lack of experimental data on the somato-dendritic distribution of channels in hilar cells. Because there was no posttraumatic increase in the amplitude of the perforant-path-evoked NMDA responses in dentate granule cells (Santhakumar et al. 2000), only AMPA receptors were included in the

network. Additionally, metabotropic receptors and electrical coupling between granule cells (MacVicar and Dudek 1982) were not included. Another simplification was to neglect the effects of synaptic failure rates, receptor desensitization and frequency-dependent facilitation, and depression at the normal (Harney and Jones 2002; Kraushaar and Jonas 2000) and sprouted synapses (Feng et al. 2003) in the dentate gyrus. Because the nature of short-term plasticity at several synapses in the network, including the synapses to and from mossy cells, are not known, more experimental data will be necessary before we can include synaptic facilitation and depression in the model networks. Future work can develop this network further also by increasing the number of cells, by incorporating fitted axonal distributions instead of the uniform distribution adopted in this study, and by including other interneuronal subtypes like the molecular layer (MOPP) and hilar commissural associational pathway (HICAP) interneurons, particularly when more data on their intrinsic properties become known. However, given the robustness of the major findings, it is unlikely that the simplifications adopted in this study would alter the basic conclusions about the contribution of mossy fiber sprouting, axonal topography, and mossy cells to network hyperexcitability.

Implications for epileptogenesis

The mossy fiber sprouting and hilar cell loss seen after concussive head injury in animal models also occur in TLE patients, including those with a history of head injury (Jeub et al. 1999; Mathern et al. 1995). Our simulations show a correlation between the degree of mossy fiber sprouting and the average number and duration of firing in the dentate granule cells and other cells. These results are in general agreement with experimental observations reporting a high degree of mossy fiber sprouting in animals that had a higher frequency of seizures (Mathern et al. 1997; Wenzel et al. 2000), although the existence and degree of association between sprouting and seizure frequency/duration in animal models are still controversial (reviewed in Nadler 2003). It is likely that the overall network behavior after sprouting and cell loss in the biological situation is modified by a number of concurrent changes, including alterations in the release of neurotransmitters (Chen et al. 1999), changes in receptor subtypes (Brooks-Kayal et al. 1998; Coulter 2001), and modifications in ion channels and pumps in both principal cells and interneurons (Chen et al. 2001; Ross and Soltesz 2000). Also, the sprouted mossy fibers could further modify network behavior by co-releasing GABA (Gutierrez 2002; Walker et al. 2001) and zinc (Buhl et al. 1996; Molnar and Nadler 2001) in addition to glutamate.

The dentate gyrus has been proposed to play an important role in curtailing the propagation of network activity in the hippocampus. It is thought that pathological processes that increase excitability or decrease inhibition compromise the dentate "gatekeeper" function and permit seizure propagation through the network (Coulter 2000; Heinemann et al. 1992; Lothman et al. 1992). Our simulations predict that moderate mossy fiber sprouting is sufficient to compromise the dentate gate and permit the spread of network activity. The restricted, lamellar distribution of sprouted mossy fiber axons, especially in the early stages of mossy fiber sprouting, might assist in the initiation of focal hyperexcitability in response to entorhinal

input. Although an intact inhibitory circuit limited the duration of self-sustained granule cell firing, the presence of mossy fiber sprouting still resulted in increased spread of focal excitation even in networks with GABAergic inhibition. The increase in network synchrony in the disinhibited network in the presence of sprouting is consistent with experimental results demonstrating that blocking inhibition increases the synchrony of recurrent excitatory postsynaptic potentials in CA3 (Miles and Wong 1986, 1987). Finally, although mossy cell loss might contribute to dentate hyperexcitability by promoting mossy fiber sprouting (Houser 1999; Masukawa et al. 1999), our simulations show that mossy cell loss is neither necessary nor sufficient to increase network excitability because deletion of mossy cells resulted in decreased excitability in the model networks in agreement with recent experimental data (Ratzliff et al. 2004).

ACKNOWLEDGMENTS

The authors thank Drs. Marco Capogna, Mathew V. Jones, and Angharad Thomas for data on paired recordings from hilar cells and granule cells and Drs. Bala Chidambaram, Jonas Dyhrfeld-Johnsen, Csaba Foldy, Allyson Howard, Michael Hines, and Robert Morgan for discussions and advice.

GRANTS

This work was funded by National Institute of Neurological Disorders and Stroke Grant NS-35915 to I. Soltesz.

REFERENCES

- Aaron GB and Dichter MA.** Excitatory synapses from CA3 pyramidal cells onto neighboring pyramidal cells differ from those onto inhibitory interneurons. *Synapse* 42: 199–202, 2001.
- Acsady L, Kamondi A, Sik A, Freund T, and Buzsaki G.** GABAergic cells are the major postsynaptic targets of mossy fibers in the rat hippocampus. *J Neurosci* 18: 3386–3403, 1998a.
- Acsady L, Katona I, Buzsaki G, and Freund TF.** Selective perisomatic innervation of hilar interneurons and mossy cells by local gabaergic afferents. *Eur J Neurosci* 10: 41, 1998b.
- Amaral DGA.** Golgi study of cell types in the hilar region of the hippocampus in the rat. *J Comp Neurol* 182: 851–914, 1978.
- Annegers JF and Coan SP.** The risks of epilepsy after traumatic brain injury. *Seizure* 9: 453–457, 2000.
- Aradi I and Holmes WR.** Role of multiple calcium and calcium-dependent conductances in regulation of hippocampal dentate granule cell excitability. *J Comput Neurosci* 6: 215–235, 1999.
- Aradi I and Soltesz I.** Modulation of network behaviour by changes in variance in interneuronal properties. *J Physiol* 538: 227–251, 2002.
- Bartos M, Vida I, Frotscher M, Geiger JR, and Jonas P.** Rapid signaling at inhibitory synapses in a dentate gyrus interneuron network. *J Neurosci* 21: 2687–2698, 2001.
- Bikson M, Hahn PJ, Fox JE, and Jefferys JG.** Depolarization block of neurons during maintenance of electrographic seizures. *J Neurophysiol* 90: 2402–2408, 2003.
- Brooks-Kayal AR, Shumate MD, Jin H, Rikhter TY, and Coulter DA.** Selective changes in single cell GABA(A) receptor subunit expression and function in temporal lobe epilepsy. *Nat Med* 4: 1166–1172, 1998.
- Brunton C.** *The Neuropathology of Temporal Lobe Epilepsy*. New York: Oxford Univ. Press, 1988.
- Buckmaster PS and Dudek FE.** Neuron loss, granule cell axon reorganization, and functional changes in the dentate gyrus of epileptic kainate-treated rats. *J Comp Neurol* 385: 385–404, 1997.
- Buckmaster PS and Dudek FE.** In vivo intracellular analysis of granule cell axon reorganization in epileptic rats. *J Neurophysiol* 81: 712–721, 1999.
- Buckmaster PS, Strowbridge BW, Kunkel DD, Schmiede DL, and Schwartzkroin PA.** Mossy cell axonal projections to the dentate gyrus molecular layer in the rat hippocampal slice. *Hippocampus* 2: 349–362, 1992.
- Buckmaster PS, Strowbridge BW, and Schwartzkroin PA.** A comparison of rat hippocampal mossy cells and CA3c pyramidal cells. *J Neurophysiol* 70: 1281–1299, 1993.

- Buckmaster PS, Wenzel HJ, Kunkel DD, and Schwartzkroin PA.** Axon arbors and synaptic connections of hippocampal mossy cells in the rat in vivo. *J Comp Neurol* 366: 271–292, 1996.
- Buckmaster PS, Yamawaki R, and Zhang GF.** Axon arbors and synaptic connections of a vulnerable population of interneurons in the dentate gyrus in vivo. *J Comp Neurol* 445: 360–373, 2002a.
- Buckmaster PS, Zhang GF, and Yamawaki R.** Axon sprouting in a model of temporal lobe epilepsy creates a predominantly excitatory feedback circuit. *J Neurosci* 22: 6650–6658, 2002b.
- Buhl EH, Otis TS, and Mody I.** Zinc-induced collapse of augmented inhibition by GABA in a temporal lobe epilepsy model. *Science* 271: 369–373, 1996.
- Bush PC, Prince DA, and Miller KD.** Increased pyramidal excitability and NMDA conductance can explain posttraumatic epileptogenesis without disinhibition: a model. *J Neurophysiol* 82: 1748–1758, 1999.
- Chen K, Aradi I, Thon N, Eghbal-Ahmadi M, Baram TZ, and Soltesz I.** Persistently modified h-channels after complex febrile seizures convert the seizure-induced enhancement of inhibition to hyperexcitability. *Nat Med* 7: 331–337, 2001.
- Chen K, Baram TZ, and Soltesz I.** Febrile seizures in the developing brain result in persistent modification of neuronal excitability in limbic circuits. *Nat Med* 5: 888–894, 1999.
- Collingridge GL, Gage PW, and Robertson B.** Inhibitory post-synaptic currents in rat hippocampal CA1 neurons. *J Physiol* 356: 551–564, 1984.
- Coulter DA.** Chronic epileptogenic cellular alterations in the limbic system after status epilepticus. *Epilepsia* 40, Suppl 1: S23–33, 1999.
- Coulter DA.** Mossy fiber zinc and temporal lobe epilepsy: pathological association with altered “epileptic” gamma-aminobutyric acid A receptors in dentate granule cells. *Epilepsia* 41 Suppl 6: S96–99, 2000.
- Coulter DA.** Epilepsy-associated plasticity in gamma-aminobutyric acid receptor expression, function, and inhibitory synaptic properties. *Int Rev Neurobiol* 45: 237–252, 2001.
- Coulter DA, Rafiq A, Shumate M, Gong QZ, DeLorenzo RJ, and Lyeth BG.** Brain injury-induced enhanced limbic epileptogenesis: anatomical and physiological parallels to an animal model of temporal lobe epilepsy. *Epilepsy Res* 26: 81–91, 1996.
- Desmond NL and Levy WB.** Granule cell dendritic spine density in the rat hippocampus varies with spine shape and location. *Neurosci Lett* 54: 219–224, 1985.
- Destexhe A, Rudolph M, Fellous JM, and Sejnowski TJ.** Fluctuating synaptic conductances recreate in vivo-like activity in neocortical neurons. *Neuroscience* 107: 13–24, 2001.
- Feng L, Molnar P, and Nadler JV.** Short-term frequency-dependent plasticity at recurrent mossy fiber synapses of the epileptic brain. *J Neurosci* 23: 5381–5390, 2003.
- Foldy C, Aradi I, Howard A, and Soltesz I.** Diversity beyond variance: modulation of firing rates and network coherence by GABAergic subpopulations. *Eur J Neurosci* 19: 119–130, 2004.
- Freund TF and Buzsáki G.** Interneurons of the hippocampus. *Hippocampus* 6: 347–470, 1996.
- Fricke RA and Prince DA.** Electrophysiology of dentate gyrus granule cells. *J Neurophysiol* 51: 195–209, 1984.
- Geiger JR, Lubke J, Roth A, Frotscher M, and Jonas P.** Submillisecond AMPA receptor-mediated signaling at a principal neuron–interneuron synapse. *Neuron* 18: 1009–1023, 1997.
- Golarai G, Greenwood AC, Feeney DM, and Connor JA.** Physiological and structural evidence for hippocampal involvement in persistent seizure susceptibility after traumatic brain injury. *J Neurosci* 21: 8523–8537, 2001.
- Gutierrez R.** Activity-dependent expression of simultaneous glutamatergic and GABAergic neurotransmission from the mossy fibers in vitro. *J Neurophysiol* 87: 2562–2570, 2002.
- Hama K, Arii T, and Kosaka T.** Three-dimensional organization of neuronal and glial processes: high voltage electron microscopy. *Microsc Res Tech* 29: 357–367, 1994.
- Harney SC and Jones MV.** Pre- and postsynaptic properties of somatic and dendritic inhibition in dentate gyrus. *Neuropharmacology* 43: 584–594, 2002.
- Heinemann U, Beck H, Dreier JP, Ficker E, Stabel J, and Zhang CL.** The dentate gyrus as a regulated gate for the propagation of epileptiform activity. *Epilepsy Res Suppl* 7: 273–280, 1992.
- Hines ML and Carnevale NT.** The NEURON simulation environment. *Neural Comput* 9: 1179–1209, 1997.
- Houser CR.** Neuronal loss and synaptic reorganization in temporal lobe epilepsy. *Adv Neurol* 79: 743–761, 1999.
- Ishizuka S and Kosaka T.** Physiological properties of mouse hippocampal mossy cells. *Neuroreport* 9: 193–199, 1998.
- Jennett B.** *Epilepsy After Nonmissile Head Injuries*. London: Heinemann, 1975.
- Jeub M, Lie A, Blumcke I, Elger CE, and Beck H.** Loss of dynorphin-mediated inhibition of voltage-dependent Ca²⁺ currents in hippocampal granule cells isolated from epilepsy patients is associated with mossy fiber sprouting. *Neuroscience* 94: 465–471, 1999.
- Johnston D, Magee JC, Colbert CM, and Christie BR.** Active properties of neuronal dendrites. *Annu Rev Neurosci* 19: 165–186, 1996.
- Kneisler TB and Dingledine R.** Spontaneous and synaptic input from granule cells and the perforant path to dentate basket cells in the rat hippocampus. *Hippocampus* 5: 151–164, 1995a.
- Kneisler TB and Dingledine R.** Synaptic input from CA3 pyramidal cells to dentate basket cells in rat hippocampus. *J Physiol* 487: 125–146, 1995b.
- Kraushaar U and Jonas P.** Efficacy and stability of quantal GABA release at a hippocampal interneuron–principal neuron synapse. *J Neurosci* 20: 5594–5607, 2000.
- Lawrence JJ, Grinspan ZM, and McBain CJ.** Quantal transmission at mossy fiber targets in the CA3 region of the rat hippocampus. *J Physiol* 554: 175–193, 2004.
- Lothman EW, Stringer JL, and Bertram EH.** The dentate gyrus as a control point for seizures in the hippocampus and beyond. *Epilepsy Res Suppl* 7: 301–313, 1992.
- Lowenstein DH, Thomas MJ, Smith DH, and McIntosh TK.** Selective vulnerability of dentate hilar neurons following traumatic brain injury: a potential mechanistic link between head trauma and disorders of the hippocampus. *J Neurosci* 12: 4846–4853, 1992.
- Lubke J, Frotscher M, and Spruston N.** Specialized electrophysiological properties of anatomically identified neurons in the hilar region of the rat fascia dentata. *J Neurophysiol* 79: 1518–1534, 1998.
- Lytton WW, Hellman KM, and Sutula TP.** Computer models of hippocampal circuit changes of the kindling model of epilepsy. *Artif Intell Med* 13: 81–97, 1998.
- MacVicar BA, and Dudek FE.** Electrotonic coupling between granule cells of rat dentate gyrus: physiological and anatomical evidence. *J Neurophysiol* 47: 579–592, 1982.
- Maex R and De Schutter E.** Resonant synchronization in heterogeneous networks of inhibitory neurons. *J Neurosci* 23: 10503–10514, 2003.
- Magee JC.** Dendritic integration of excitatory synaptic input. *Nat Rev Neurosci* 1: 181–190, 2000.
- Margerison JH and Corsellis JA.** Epilepsy and the temporal lobes. A clinical, electroencephalographic and neuropathological study of the brain in epilepsy, with particular reference to the temporal lobes. *Brain* 89: 499–530, 1966.
- Masukawa LM, Burdette LJ, McGonigle P, Wang H, O'Connor W, Sperling MR, O'Connor MJ, and Uruno K.** Physiological and anatomical correlates of the human dentate gyrus: consequences or causes of epilepsy. *Adv Neurol* 79: 781–794, 1999.
- Mathern GW, Bertram EH, III, Babb TL, Pretorius JK, Kuhlman PA, Spradlin S, and Mendoza D.** In contrast to kindled seizures, the frequency of spontaneous epilepsy in the limbic status model correlates with greater aberrant fascia dentata excitatory and inhibitory axon sprouting, and increased staining for N-methyl-D-aspartate, AMPA and GABA(A) receptors. *Neuroscience* 77: 1003–1019, 1997.
- Mathern GW, Pretorius JK, and Babb TL.** Influence of the type of initial precipitating injury and at what age it occurs on course and outcome in patients with temporal lobe seizures. *J Neurosurg* 82: 220–227, 1995.
- Migliore M, Cook EP, Jaffe DB, Turner DA, and Johnston D.** Computer simulations of morphologically reconstructed CA3 hippocampal neurons. *J Neurophysiol* 73: 1157–1168, 1995.
- Miles R and Wong RK.** Excitatory synaptic interactions between CA3 neurones in the guinea pig hippocampus. *J Physiol* 373: 397–418, 1986.
- Miles R and Wong RK.** Inhibitory control of local excitatory circuits in the guinea pig hippocampus. *J Physiol* 388: 611–629, 1987.
- Molnar P and Nadler JV.** Mossy fiber-granule cell synapses in the normal and epileptic rat dentate gyrus studied with minimal laser photostimulation. *J Neurophysiol* 82: 1883–1894, 1999.
- Molnar P and Nadler JV.** Synaptically-released zinc inhibits N-methyl-D-aspartate receptor activation at recurrent mossy fiber synapses. *Brain Res* 910: 205–207, 2001.
- Mott DD, Turner DA, Okazaki MM, and Lewis DV.** Interneurons of the dentate-hilus border of the rat dentate gyrus: morphological and electrophysiological heterogeneity. *J Neurosci* 17: 3990–4005, 1997.

- Nadler JV.** The recurrent mossy fiber pathway of the epileptic brain. *Neurochem Res* 28: 1649–1658, 2003.
- Nissinen JPT, Kharatishvili I, McIntosh TK, and Pitkänen A.** Epileptogenesis induced by traumatic brain injury in rats. *Epilepsia* 44:175, 2003.
- Patton PE and McNaughton B.** Connection matrix of the hippocampal formation: I. The dentate gyrus. *Hippocampus* 5: 245–286, 1995.
- Rall W, Burke RE, Holmes WR, Jack JJ, Redman SJ, and Segev I.** Matching dendritic neuron models to experimental data. *Physiol Rev* 72: S159–186, 1992.
- Ratzliff AH, Howard AL, Santhakumar V, Osapay I, and Soltesz I.** Rapid deletion of mossy cells does not result in a hyperexcitable dentate gyrus: implications for epileptogenesis. *J Neurosci* 24: 2259–2269, 2004.
- Ratzliff AH, Santhakumar V, Howard A, and Soltesz I.** Mossy cells in epilepsy: rigor mortis or vigor mortis? *Trends Neurosci* 25: 140–144, 2002.
- Ross ST and Soltesz I.** Selective depolarization of interneurons in the early posttraumatic dentate gyrus: involvement of the Na(+)/K(+)-ATPase. *J Neurophysiol* 83: 2916–2930, 2000.
- Santhakumar V, Bender R, Frotscher M, Ross ST, Hollrigel GS, Toth Z, and Soltesz I.** Granule cell hyperexcitability in the early post-traumatic rat dentate gyrus: the “irritable mossy cell” hypothesis. *J Physiol* 524: 117–134, 2000.
- Santhakumar V, Ratzliff AD, Jeng J, Toth K, and Soltesz I.** Long-term hyperexcitability in the hippocampus after experimental head trauma. *Ann Neurol* 50: 708–717, 2001.
- Santhakumar V, Voipio J, Kaila K, and Soltesz I.** Post-traumatic hyperexcitability is not caused by impaired buffering of extracellular potassium. *J Neurosci* 23: 5865–5876, 2003.
- Scharfman HE.** Characteristics of spontaneous and evoked EPSPs recorded from dentate spiny hilar cells in rat hippocampal slices. *J Neurophysiol* 70: 742–757, 1993.
- Scharfman HE.** Dentate hilar cells with dendrites in the molecular layer have lower thresholds for synaptic activation by perforant path than granule cells. *J Neurosci* 11: 1660–1673, 1991.
- Scharfman HE.** Electrophysiological evidence that dentate hilar mossy cells are excitatory and innervate both granule cells and interneurons. *J Neurophysiol* 74: 179–194, 1995.
- Scharfman HE, Smith KL, Goodman JH, and Sollas AL.** Survival of dentate hilar mossy cells after pilocarpine-induced seizures and their synchronized burst discharges with area CA3 pyramidal cells. *Neuroscience* 104: 741–759, 2001.
- Sik A, Penttonen M, and Buzsáki G.** Interneurons in the hippocampal dentate gyrus: an in vivo intracellular study. *Eur J Neurosci* 9: 573–588, 1997.
- Sloviter RS.** Permanently altered hippocampal structure, excitability, and inhibition after experimental status epilepticus in the rat: the “dormant basket cell” hypothesis and its possible relevance to temporal lobe epilepsy. *Hippocampus* 1: 41–66, 1991.
- Sloviter RS.** The functional organization of the hippocampal dentate gyrus and its relevance to the pathogenesis of temporal lobe epilepsy. *Ann Neurol* 35: 640–654, 1994.
- Sloviter RS, Zappone CA, Harvey BD, Bumanglag AV, Bender RA, and Frotscher M.** “Dormant basket cell” hypothesis revisited: relative vulnerabilities of dentate gyrus mossy cells and inhibitory interneurons after hippocampal status epilepticus in the rat. *J Comp Neurol* 459: 44–76, 2003.
- Staley KJ, Otis TS, and Mody I.** Membrane properties of dentate gyrus granule cells: comparison of sharp microelectrode and whole-cell recordings. *J Neurophysiol* 67: 1346–1358, 1992.
- Sutula T, Cascino G, Cavazos J, Parada I, and Ramirez L.** Mossy fiber synaptic reorganization in the epileptic human temporal lobe. *Ann Neurol* 26: 321–330, 1989.
- Sutula TP, Golarai G, and Cavazos J.** Assessing the functional significance of mossy fiber sprouting. *Epilepsy Res Suppl* 7: 251–259, 1992.
- Toth Z, Hollrigel GS, Gorcs T, and Soltesz I.** Instantaneous perturbation of dentate interneuronal networks by a pressure wave-transient delivered to the neocortex. *J Neurosci* 17: 8106–8117, 1997.
- Traub RD, Jefferys JG, and Whittington MA.** Enhanced NMDA conductance can account for epileptiform activity induced by low Mg^{2+} in the rat hippocampal slice. *J Physiol* 478: 379–393, 1994.
- Traub RD, Knowles WD, Miles R, and Wong RK.** Models of the cellular mechanism underlying propagation of epileptiform activity in the CA2–CA3 region of the hippocampal slice. *Neuroscience* 21: 457–470, 1987.
- Walker MC, Ruiz A, and Kullmann DM.** Monosynaptic GABAergic signaling from dentate to CA3 with a pharmacological and physiological profile typical of mossy fiber synapses. *Neuron* 29: 703–715, 2001.
- Wang XJ, Tegner J, Constantinidis C, and Goldman-Rakic PS.** Division of labor among distinct subtypes of inhibitory neurons in a cortical microcircuit of working memory. *Proc Natl Acad Sci USA* 101: 1368–1373, 2004.
- Wenzel HJ, Buckmaster PS, Anderson NL, Wenzel ME, and Schwartzkroin PA.** Ultrastructural localization of neurotransmitter immunoreactivity in mossy cell axons and their synaptic targets in the rat dentate gyrus. *Hippocampus* 7: 559–570, 1997.
- Wenzel HJ, Woolley CS, Robbins CA, and Schwartzkroin PA.** Kainic acid-induced mossy fiber sprouting and synapse formation in the dentate gyrus of rats. *Hippocampus* 10: 244–260, 2000.
- White JA, Chow CC, Ritt J, Soto-Trevino C, and Kopell N.** Synchronization and oscillatory dynamics in heterogeneous, mutually inhibited neurons. *J Comput Neurosci* 5: 5–16, 1998.
- Zhang N and Houser CR.** Ultrastructural localization of dynorphin in the dentate gyrus in human temporal lobe epilepsy: a study of reorganized mossy fiber synapses. *J Comp Neurol* 405: 472–490, 1999.